

**TOWARDS SYSTEM IDENTIFICATION USING SINGLE
CHANNEL MEASUREMENT IN WIRELESS SENSING
NETWORK**

by

Malek Lazhari

A thesis

submitted to the Faculty of Graduate Studies

in partial fulfilment of the requirement for the

degree of Master of Science

in

Civil Engineering

Lakehead University

Thunder Bay, Ontario

May 2018

© Malek Lazhari, 2018

Dedicated to my parents and my wife

Table of Contents

List of Tables	v
List of Figures	ix
Abstract	x
Acknowledgements	xii
Chapter 1 Introduction	2
1.1 Condition Assessment of Structure	2
1.2 Wireless and Mobile Sensing Technology	4
1.3 Literature Review of System Identification	9
1.3.1 Time-domain Methods	10
1.3.2 Frequency-domain Methods	11
1.3.3 Time-frequency domain Methods	12
1.4 Gap Areas of Existing Literature	15
1.5 Thesis Objectives	16
Chapter 2 Proposed Method	18
2.1 Background	18
2.1.1 Empirical Mode Decomposition	19
2.1.2 Time-Varying Filtering-based EMD	22
2.2 Proposed Methodology	30
Chapter 3 Numerical Study	33
3.1 3-DOF Model	33
3.2 4-DOF Model	42

3.3	10-DOF Model	48
Chapter 4	Experimental and Full-scale Studies	55
4.1	Experimental Study	55
4.2	Full-scale Study	62
Chapter 5	Conclusions and Recommendations	69
5.1	Conclusions	69
5.2	Major Contributions	70
5.3	Future Work	70
Bibliography	72

List of Tables

Table 1	List of acronyms	1
Table 3.1	Theoretical and identified modal parameters of the 3-DOF model	39
Table 3.2	Theoretical and identified modal parameters of the 4-DOF model	45
Table 3.3	Theoretical and identified modal parameters of second floor measurement	54
Table 4.1	Theoretical and identified modal parameters of the experimental model	62
Table 4.2	Theoretical and identified modal parameters of the footbridge .	66

List of Figures

Figure 1.1	Key steps of SHM	3
Figure 1.2	(a) Traditional (centralized) vs. (b) decentralized sensing network [5]	5
Figure 1.3	Mobile sensors [14, 15]	7
Figure 1.4	Mobile sensing network [4]: (a) under a horizontal element, (b) above horizontal element and (c) on a vertical element	7
Figure 1.5	System identification	10
Figure 2.1	Original sine signals, their mixed signal and Fourier spectrum	21
Figure 2.2	IMFs of $y(t)$ and its Fourier spectrum	22
Figure 2.3	Original sine signals, their mixed signal and Fourier spectrum under 0% noise	25
Figure 2.4	The IMFs and its Fourier spectrum under 0% noise	25
Figure 2.5	Mixed signal and its corresponding Fourier spectrum under 5% noise	26
Figure 2.6	The IMFs and its Fourier spectrum under 5% noise	27
Figure 2.7	Mixed signal and its corresponding Fourier spectrum under 10% noise	27
Figure 2.8	The IMFs and its Fourier spectrum under 10% noise	28
Figure 2.9	Mixed signal and its corresponding Fourier spectrum under 5% noise	29
Figure 2.10	The IMFs and its Fourier spectrum under 5% noise	29
Figure 2.11	Time domain data and corresponding Fourier spectrum	30

Figure 2.12	The IMFs and its Fourier spectrum under 10% noise	30
Figure 2.13	Flowchart of the proposed method	32
Figure 3.1	3-DOF model	33
Figure 3.2	Time-history and Fourier spectra of the ground motion	34
Figure 3.3	Time-history and Fourier spectra of floor responses	35
Figure 3.4	RMS values of IMFs of the first floor measurement	36
Figure 3.5	Cluster of frequencies of (a) all IMFs and (b) IMFs that are above μ_{rms} in the first floor measurement	36
Figure 3.6	IMFs of the first floor measurement obtained from the TVF-EMD method	37
Figure 3.7	RMS values of IMFs of the second floor measurement	38
Figure 3.8	Cluster of frequencies of (a) all IMFs and (b) IMFs that are above μ_{rms} in the second floor measurement	38
Figure 3.9	IMFs of the second floor measurement obtained from the TVF-EMD	39
Figure 3.10	RMS values of IMFs of the third floor measurement	40
Figure 3.11	Cluster of frequencies of (a) all IMFs and (b) IMFs that are above μ_{rms} in the third floor measurement	40
Figure 3.12	IMFs of the third floor measurement obtained from the TVF-EMD	41
Figure 3.13	Damping ratio of the resulting modal responses of second floor measurement	41
Figure 3.14	4-DOF model	42
Figure 3.15	Fourier spectra of floor vibration measurements	42
Figure 3.16	RMS values of IMFs of measurement at first DOF	43

Figure 3.17 Cluster of frequencies of (a) all IMFs and (b) IMFs that are above μ_{rms} in the measurement at first DOF	44
Figure 3.18 IMFs of the measurement at first DOF obtained from the TVF-EMD method	44
Figure 3.19 RMS values of IMFs of the measurement at fourth DOF	46
Figure 3.20 Cluster of frequencies of (a) all IMFs and (b) IMFs that are above μ_{rms} in the measurement at fourth DOF	46
Figure 3.21 Fourier spectra of IMFs of the fourth floor measurement	47
Figure 3.22 Damping ratio of the resulting modal responses the of the 4th floor measurement	47
Figure 3.23 10-DOF model	48
Figure 3.24 Fourier spectra of floor vibration measurements	49
Figure 3.25 RMS values of IMFs of second floor measurement	50
Figure 3.26 Cluster of frequencies of all IMFs	50
Figure 3.27 Cluster of frequencies of IMFs that are above μ_{rms}	51
Figure 3.28 Fourier spectra of IMFs of the second floor measurement	51
Figure 3.29 RMS values of IMFs of fifth floor measurement	52
Figure 3.30 Cluster of frequencies of all IMFs	53
Figure 3.31 Cluster of frequencies of IMFs that are above μ_{rms}	53
Figure 3.32 Fourier spectra of IMFs of the fifth floor	54
Figure 4.1 Experimental model	56
Figure 4.2 The Narada unit	56
Figure 4.3 The Narada base station	56

Figure 4.4	Mobile sensing where sensor is located at (a) 5th floor, (b) 4th floor and (c) 1st floor	57
Figure 4.5	Fourier spectra of second floor vibration measurement	58
Figure 4.6	RMS values of IMFs of the second floor measurement	58
Figure 4.7	Cluster of frequencies of all IMFs	59
Figure 4.8	IMFs of the second floor measurement	59
Figure 4.9	RMS values of IMFs of the fifth floor measurement	60
Figure 4.10	Cluster of frequencies of all IMFs	61
Figure 4.11	Fourier spectra of IMFs of the fifth floor measurement	61
Figure 4.12	Pedestrian bridge on the campus of Lakehead University instrumented with wireless sensors	62
Figure 4.13	Decentralized implementation of sensors placed along the foot-bridge	63
Figure 4.14	The Narada unit at the mid-span of the bridge	64
Figure 4.15	Fourier spectra of bridge vibration measurement	64
Figure 4.16	RMS values of IMFs of the mid-span measurement	65
Figure 4.17	Cluster of frequencies of all IMFs	65
Figure 4.18	FE model and its mode shapes	67
Figure 4.19	IMFs of the mid-span vibration measurement	67
Figure 4.20	Damping ratio of the resulting modal responses of bridge	68

Abstract

In the last few years, structural health monitoring has gained significant popularity to perform real-time condition assessment of civil structures. With the aid of mobile sensing network, movable wireless sensors have made a paradigm shift in cost-effective and faster deployment of sensors in large-scale structures. A wide range of system identification methods has been developed by different researchers to accurately identify modal parameters from the measured vibration data. However, most of these techniques are suitable only when all key locations of the structures are instrumented. In the case of mobile sensing network where a sensor is autonomously moved from one location to another, only a few sensors are available at any time. In this research, a newer time-frequency method, namely the empirical mode decomposition (EMD), is explored and improved to conduct system identification using single channel measurement.

The original EMD method results in significant mode-mixing in the modal responses when utilizing closely-spaced modes and data with measurement noise. In this thesis, time-varying filtering based empirical mode decomposition (TVF-EMD) is proposed to undertake ambient modal identification. The proposed method is fully adaptive and suitable for automation since it uses only one channel of data at a time. An energy-based thresholding criterion is proposed to identify dominant frequency components of the vibration data. Once the key signal components are identified, a cluster diagram is integrated with TVF-EMD to identify modal responses that are utilized for modal identification. Such modification shows improved performance of the

TVF-EMD in identifying modal parameters using single channel measurement under a wide-range of challenging situations including closely-spaced modes and measurement noise. The proposed method is verified using a suite of numerical, experimental and full-scale studies using wireless sensors in a decentralized manner. The proposed methodology shows significant potential towards its application in modern mobile and robotic sensors.

Acknowledgements

I would like to express my heartiest thanks and gratitude to my thesis research supervisor, Dr. Ayan Sadhu, for his inspirational guidance, constructive feedback and valuable support. Dr. Sadhu has been a wonderful mentor and has provided me with the positive attitude and continuous motivation to pursue my research in such an interesting topic.

I sincerely thank Dr. Jian Deng and Dr. Meilan Liu for kindly serving on my thesis committee. I would like to thank Tripoli University and Libyan Ministry of Education for their valuable financial support throughout my graduate studies at Lakehead University. I really appreciate my research teammates (Peter Friesen, Mohamed Barbosh, Nawaf Almasri, Chanakya Bodupalli and Sandeep Sony) for their continuous support and encouragement during my stay at Lakehead University. Special thanks are reserved to Nawaf Almasri for his assistance in wireless sensors used in this thesis. I would like to thank a group of undergraduate degree project students (Hon Yin Cheng, Ian Dornbush, Jason Guenther, and Landon Little) who assisted in the data collection of footbridge located in the campus of Lakehead University.

Finally, I express my profound gratitude to my parents, wife and son (Mohamed) for their continuous encouragement throughout my journey at Lakehead University. This accomplishment would not have been possible without the unfailing support of my family.

Acronyms

Following is the list of all relevant acronyms used in this thesis.

Table 1: List of acronyms

EMD	Empirical mode decomposition
TVF-EMD	Time-varying filtering EMD
SHM	Structural health monitoring
MSN	Mobile sensing network
WSN	Wireless sensing network
SI	System identification
CE	Complex exponential
SSI	Stochastic subspace identification
FDD	Frequency domain decomposition
WT	Wavelet transform
BSS	Blind source separation
IMF	Intrinsic mode function
NE _x T	Natural excitation technique
RD	EMD-based random decrement
VMD	Variational mode decomposition
MEMD	Multivariate empirical mode decomposition
ICA	Independent component analysis
DOF	Degrees-of-freedom
RMS	Root-mean-square
FE	Finite element

Chapter 1

Introduction

In this chapter, condition assessment of structure and its overall importance in monitoring of large-scale infrastructure is introduced. Structural health monitoring (SHM) requires rich vibration data collected from structures under in-service condition. Once data are collected, system identification is conducted to extract useful information of the structure. Recent development of decentralized wireless sensing network followed by mobile sensing approaches has shown a paradigm shift in modern data collection technology. A brief overview of mobile sensing network (MSN) is discussed in light of decentralized health monitoring techniques. While discussing this, potential challenges of system identification in MSN are identified to establish the gap areas of this research. Limitations of existing system identification methods are next discussed followed by organization of key research objectives proposed in this thesis.

1.1 Condition Assessment of Structure

Large-scale civil infrastructure including bridges, buildings, wind turbines, retaining walls, and towers may lose structural integrity due to exposure to extreme loads such as strong winds, floods, fires, earthquakes, and traffic loads. If progression of damage is unattended over a period of time, these structures can suffer long-term damage, even a catastrophic failure in the near future. Typical examples of deterioration are corrosion, wood decay, fatigue, spalling and delamination of concrete, foundation

settlement, and vibrations from adjacent construction. Structural Health Monitoring (SHM) is an important tool to evaluate current condition of the structure and predict future damage. It can reduce the overall repair and maintenance cost by detecting and measuring early damages when they occur. Through continuously monitoring of the existing structural condition in a timely manner, SHM can effectively mitigate long-term damage [1]. The main idea of system identification is to detect damage by discovering the change in structural parameters such as stiffnesses and frequencies through the model responses of the structure based on the measured vibration data.

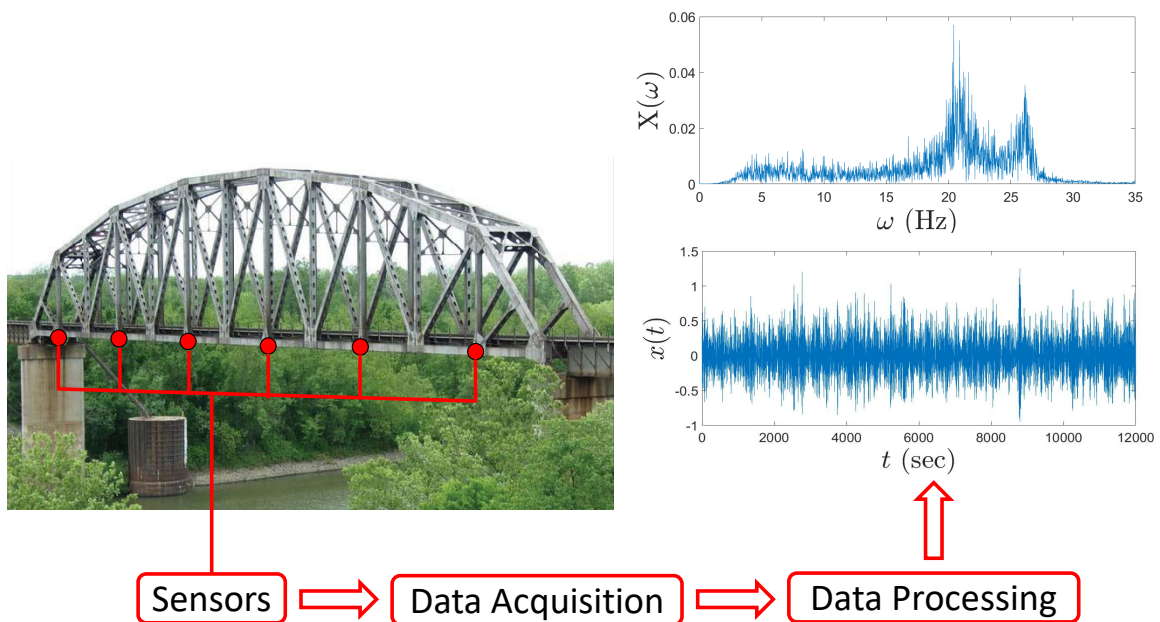


Figure 1.1: Key steps of SHM

SHM is accomplished using four key steps which are data collection followed by system identification and condition assessment, finally making a decision about the maintenance and retrofitting as shown in Fig. 1.1. Traditional approaches of data collection involve attachment of wired sensors to the structures which are then monitored through oncoming data (i.e., acceleration and displacement). The collected

data is processed by using system identification techniques [2] to estimate system parameters (i.e., frequencies, damping and mode shapes) and evaluate current condition of the structure. Recently, wireless sensors have become a promising technique in the field of SHM as it is relatively inexpensive and easier to install compared to wired sensors. Owing to its decentralized nature of data collection and transmission, it has gained significant popularity to the SHM community all over the world. Extending this concept using robots and movable vehicles, mobile sensing approach has garnered potential attention where wireless sensors or cameras are attached to a robot or vehicle and used for data transmission and data processing, wirelessly.

1.2 Wireless and Mobile Sensing Technology

In recent years, wireless sensing network (WSN) [3] has offered easier and feasible solution to collect good quality vibration data and estimate dynamical properties of structures. It has potentially become an efficient tool that monitors acceleration and displacement of various structures without requiring a large central data acquisition system. Unlike wired sensors, WSN is cost-effective and easier to install with fewer labors, thereby leading to substantial cost saving for the infrastructure owners. Over the past 10 years, many academic and industrial prototypes [3] have been developed and studied in laboratory and field-based applications. In general, low-cost wireless sensing units are usually required to be inserted with high-accuracy accelerometers for accurate data measurement and system identification of civil structures [4]. Once all sensor nodes are set up, each node (known as slave node) communicates with the base station (namely the master node) independently and wirelessly as shown in Fig. 1.2, thereby making data collection and acquisition decentralized [5]. Such decentralized sensing approach eliminates labor-intensive and costly cable placement, and reduce

overall maintenance costs to the infrastructure owners.

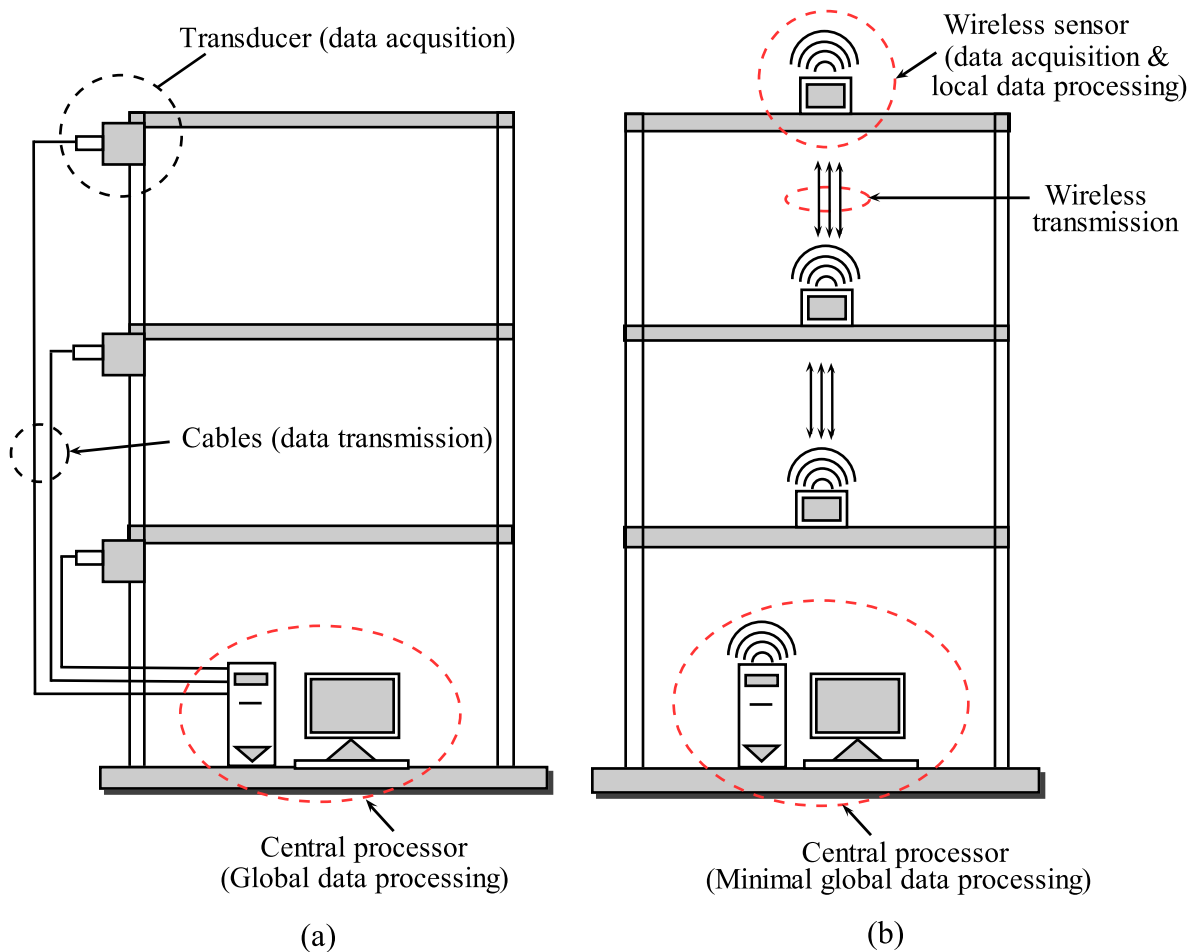


Figure 1.2: (a) Traditional (centralized) vs. (b) decentralized sensing network [5]

Expanding the concept of WSN with mobile sensors further, a mobile sensor network (MSN) is exploited to perform condition assessment of different structural systems. With recent development in robotic technology, mobile sensing can be used to perform accurate real-time data acquisition with minimal setup cost. It is considered an enhancement of wireless sensing technology that can offer higher data rates and accurate time synchronization. A mobile sensing node can be a small mobile robot being equipped with WSN that offers flexible architecture compared to static wireless sensor deployment. Apart from these sensors being cost-effective, time-saving, and

compact, it can easily be implemented with camera and wireless sensors for easy and fast data acquisition.

In recent studies, various MSNs have been utilized to monitor the performance of different civil structures. Interestingly, MSN can accomplish adaptive and high spatial resolutions with little human effort and relative few number of mobile sensor nodes [6]. This technology has efficiently shown an improved performance in the field of SHM by exploiting its potential as wireless mobile sensors. For instance, Tche et al. [7] developed a small robot with two magnetic wheels in a motorcycle arrangement to inspect internal casing of ferromagnetic pipes with complex-shaped structures. Another study [8] designed a mobile inspection robot with an automatic pipe tracking system through machine vision. Wall-climbing robots were also developed by using dry elastomer adhesion [9] or claw-gripping [10]. Some researchers integrated mobility into traditional sensors for SHM. For example, a beam-crawler was developed for wirelessly powering and debrif battery-less peak-strain sensors [11]. A robot able to creep on a 2D surface was developed for visually inspecting aircraft exterior where the robot used ultrasonic motors for mobility and suction cups for adhesion [12]. As a mobile host, a remotely controlled model helicopter was demonstrated for charging and communicating with wireless sensors [13]. Fig. 1.3 and Fig. 1.4 show different types of mobile sensors that can be attached to a robot that moves along the structural elements to collect the vibration data.

Initial development of the mobile robotic systems was carried out to develop robots for automation in construction as well as non-destructive testing (NDT) in bridges. Lorenc et al. [16] developed a robotic bridge maintenance system primarily for service inspection and maintenance of bridges. Tung et al. [17] developed a mobile manipulator image system for bridge crack inspection that was consisted of cameras,

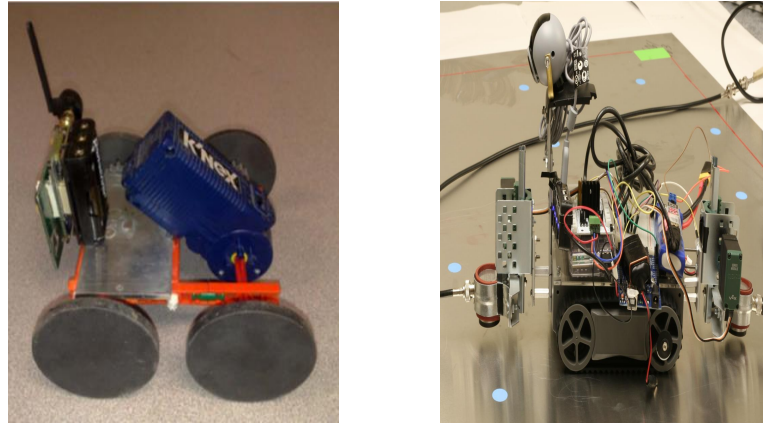


Figure 1.3: Mobile sensors [14, 15]

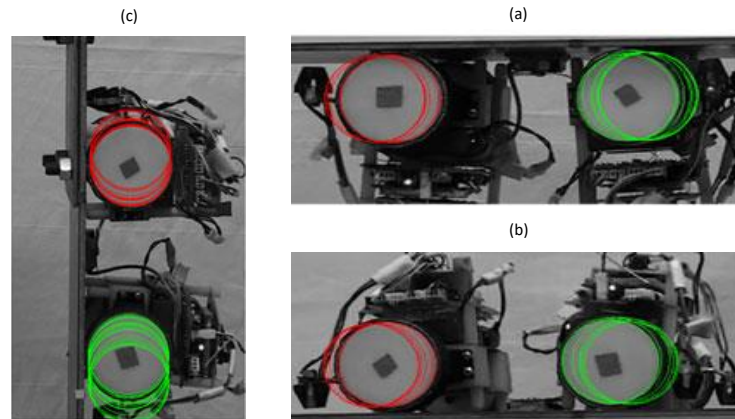


Figure 1.4: Mobile sensing network [4]: (a) under a horizontal element, (b) above horizontal element and (c) on a vertical element

and a manipulator mounted on a mobile vehicle. Few years later, Oh et al. [18] developed a seven degrees-of-freedom robotic system equipped with a hydraulic actuator system. A machine vision system was integrated into the robotic system for tracing, detecting and evaluating the dimensions of the cracks in the bridge. Zhu et al. [19] developed and validated a new mobile sensing system as a proof-of-concept study for the SHM. The proposed mobile sensing device consisted of two two-wheeled cars connected with a beam carrying the accelerometers. The goal of this study was to detect the structural damage in steel portal frame. Limll et al. [20] proposed a robotic crack inspection and mapping system for accurate assessment of cracks in the

bridges. Multiple mobile sensing systems [4] were used to collect modal parameters of pedestrian bridges wirelessly.

In the study [21], an autonomous robot was used as a mobile sensing device for inspection and evaluation of the bridge deck. The robotic system was built with electrical resistivity sensor, impact echo sensors, and the panoramic camera was mounted on a computer-controlled, extendable mast. Matarazzo et al. [22] studied the use of mobile sensors for system identification with missing observations. Stochastic state-space-based modified Kalman filtering was used to account for the missing observations in the ambient vibration data collected at the Golden Gate bridge. Recently, Goorts et al. [23] evaluated the use of a mobile sensor to understand the densification of modal coordinates instead of a broad array of wireless sensors. The mobile sensor moved over the structure and was attached with an accelerometer onto specific points where modal coordinates were required. [14] aimed at developing a deployable autonomous control system for short-term vibration mitigation. The research used an unmanned ground vehicle for accurate positioning of sensors, a modified husky A200 robot mounted with electromechanical mass damper for better control, and onboard vision sensors to facilitate self-sufficient positioning of the device as well as sensing.

Apart from their several advantages, the mobile sensing systems pose several challenges that require future advancement to make them suitable in a wide variety of SHM applications. The MSN has the following limitations in the context of SHM applications:

- These sensors require sophisticated robots and control systems through a continuous multidisciplinary collaboration of researchers from computer science, electrical engineering, mechanical engineering and civil engineering, for instance.

- The sensor in MSN does not attach directly to the structure; therefore robot-sensor interaction may significantly influence the data collected from the structure.
- MSN relies on moving sensors and deals with single channel measurement which requires development of theoretically challenging, underdetermined system identification methods.

In this thesis, the last limitation of MSN is addressed through a novel time-frequency decomposition technique. The first two aspects are reserved for future research and are not considered here. In the following section, a comprehensive review is given to identify the challenges of existing system identification method in the context of MSN and single measurement.

1.3 Literature Review of System Identification

As shown in Fig. 1.5, System Identification (SI) [24, 25] is a technique of building mathematical models from the input-output data extracted from the system. The main objective of SI is to understand the behavior of a structure and predict its performance for fault diagnosis and maintenance. SI is an important tool to evaluate the current performance or safety functions of the structure and recognize the extent of damage due to natural hazards such as earthquake, strong wind and in-service loads. SI is primarily comprised of three categories of techniques: a white box, black box, and grey box [26].

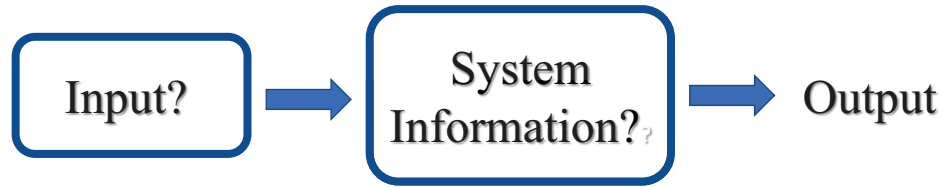


Figure 1.5: System identification

In white box modeling, the models are formulated based on simple experiments to inquire into the physical laws. In black box modeling, the model form and system behavior are entirely unknown where a model is built without any previous knowledge of the system and is entirely based only on data. The model characterizes how the outputs depend on the inputs, not on how the system actually is. Grey box modeling is an intermediate technique when peculiarities of internal laws are not entirely known. Due to unavailability of input information, black box modeling is most common method of SI for civil engineering structures. There are different output-only modal identification techniques (also known as *operational modal analysis*) [5, 27] used in both structural and mechanical system since early 19's. These methods work either in the time, frequency or time-frequency domain.

1.3.1 Time-domain Methods

Time-domain methods are among the most preliminary methods of the SI. Complex exponential (CE) algorithm [28] based on Prony's method is probably the first single-input single-output parametric identification technique among all time-domain methods [29, 30, 31, 32, 33]. Asmussen et al. [34] and Lin et al. [35] combined the Ibrahim

time-domain method with random decrement method to perform modal identification of structural system. In the early to mid 1990's [36, 37], Stochastic Subspace Identification (SSI) was developed which became a powerful tool for output-only system identification. The stochastic state space modeling was used as the framework of SSI method. In [38], vibration data were used to track the changes in stiffness, however, the study found that noise contamination and environmental changes affected the performance of the method to detect small variations in stiffness.

In [39], an optimization method was adopted to reduce the error between the moment generating function and a numerical modal of the structure to identify damage. This method used limited sensors but it required a significant user intervention. Liu et al. [40] utilized random decrement technique to analyze non-stationary response whereas Zhong et al. [41] applied recursive subspace identification to identify structural changes under non-stationary excitation. In summary, time domain methods are easier to implement. However, it is a computationally intensive and time-consuming process. Also, the generality of time domain methods requires input data which are difficult to obtain in large structures and has shown poor performance towards progressive damage detection.

1.3.2 Frequency-domain Methods

The frequency domain methods perform the vibration analysis concerning frequency, rather than time. In other words, it converts a time history into its frequency spectrum which allows the user to see frequencies that are present in the system. Frequency domain techniques are fundamentally based on frequency response functions [42, 43, 44]. Richardson et al. [42] developed a rational fraction polynomial based

method whereas a power-spectral density based on peak picking method was developed by [43]. The other popular frequency domain method called frequency domain decomposition (FDD) was developed to resolve the complexities encountered in peak picking while retaining the advantages of the traditional peak picking technique [44]. Brincker et al. [45] extended the classical FDD to identify the symmetrical structures with closely-spaced modes.

The power spectral density functions of the dynamic strain measures [46] was used to detect changes in stiffness of the structure [47]. By integrating FDD with Bayesian approach, Figueiredo et al. [48] estimated modal parameters. Ding et al. [49] addressed the problem of SI with incomplete structural information. In spite of its success, frequency domain methods are not able to detect changes in system parameters due to the fact that it localizes information only with respect to frequency. Recently, there has been a significant growth in signal processing which results in the development of robust SI methods using time-frequency decomposition techniques.

1.3.3 Time-frequency domain Methods

Time-frequency domain methods are able to give a picture of time and frequency domain variation of energy of a signal simultaneously [50, 51]. In the last two decades, time-frequency domain methods have acquired a considerable interest, particularly in civil and mechanical systems. Wavelet transform (WT) [52], blind source separation (BSS) [5] and empirical mode decomposition (EMD) [53] are used as modal identification techniques for large-scale civil infrastructure and widely used in many different fields of science and engineering. Of all methods, EMD has the capability of using only a single channel of measurement that could be utilized in MSN.

The empirical mode decomposition (EMD) is a time-frequency domain method

which is purely data-driven, does not require any basis functions, and works with nonlinear and nonstationary signal [55]. It is an adaptive time-frequency decomposition method which composes the signal into a set of oscillatory waveforms known as intrinsic mode functions (IMF). IMFs are extracted using averaging and interpolation operations. This process is known as *sifting*. However, sifting operations cause considerable mode mixing in the IMFs. Recently, many studies were conducted to solve this shortcoming. For example, Qin et al. [56] improved the EMD to solve mode-mixing problems with closely spaced frequencies. A bandwidth restricted EMD was used to decompose nonstationary output measurements with closely-spaced frequency components. The modal parameters were then obtained from intrinsic mode function (IMFs) using random decrement technique and stochastic subspace identification. Natural excitation technique (NExT) was combined with EMD with intermittency check criterion [57]. The decomposed signal was extracted by using EMD, in which the cut-off frequency separated signal from its mode-mixed signals. A new method called wavelet-bounded empirical mode decomposition was developed to solve the problem of mode mixing in EMD [58].

Zhang et al. [59] developed a frequency modulated EMD to determine the variations in the modal parameters of a bridgeair system. It overcame one of the main shortcomings of the EMD, the lack of separation of closely spaced modes. The proposed method was used to extract frequencies and damping ratio of the aero-elastic system during the free decay vibration and able to identify nonlinearity in the transient aero-elastic vibration. The modal parameters of power transformer winding were identified by an improved EMD algorithm [60]. First, an ensemble EMD was used to decompose the vibration signals. Then a masking signal was introduced to eliminate the mode-mixing with the selected masking frequency. Hell et al. [61] developed an

EMD-based random decrement (RD) technique to identify modal parameters from vibrational data. After decomposing a nonstationary measurement data to a series of quasi-stationary IMFs using EMD, RD technique was applied to the chosen IMFs to obtain the free-decay response. The proposed method was validated using the Nanjing Yangtze River Bridge. In another study [62], the bridge frequencies of higher modes were extracted in some steps. Yu et al. [63] combined EMD with SSI to estimate modal parameters of a slender bridge. Another derivative of EMD was recently proposed as variational mode decomposition (VMD) that addressed the weaknesses of the EMD method. The efficiency of the algorithm was evaluated by a series of numerical, laboratory, and field case studies [64].

Lately, a new method called multivariate empirical mode decomposition (MEMD) was developed as a modal identification tool that can deal with multisensor vibration measurements of civil structures [65, 66, 67]. To alleviate mode mixing, ensemble EMD [68] and Independent Component Analysis (ICA) method [69] were respectively integrated with the MEMD. The performance of MEMD was evaluated using several numerical, experimental and full-scale studies.

Apart from modal identification, Li et al. [70] combined EMD and wavelet transform (WT) for damage detection of civil structures. Once the mono-component signals were extracted by the EMD, the exact location and extent of damage were identified using the WT. The proposed method was validated using the numerical simulation and a four-story shear structure building to harmonic excitation. Xu et al. [71] presented a damage detection algorithm utilizing EMD where the structural damage was simulated by suddenly releasing pre-tensioned springs simultaneously. Then EMD was applied to the measured time histories to identify damage time instant and location for different experiments. In [72], EMD was integrated with

Hilbert transform to perform structural health monitoring of civil structures. The method processed time-series measurement from the structure without damage and with damage. In another research [73], the EMD method was applied for bridge damage detection of a passing vehicle. A variation in the acceleration signals of healthy and corresponding damaged structures was used to identify the damage location in the presence of a road. EMD was also explored for damage detection by identifying stiffness change from a localized feature in the traffic-induced structural response. However, the effectiveness of this technique is limited by the roughness of the road profile, the vehicle speed, and the noise level [74]. A method based on the lamb wave mode and EMD was proposed on a composite material plate structures damaged by the impact. In another study, Guo et al. [75] utilized EMD for fault detection of water pipeline.

1.4 Gap Areas of Existing Literature

- In mobile sensing technology, a sensor is attached to the robot that can move along the structure. In such sensing framework, at any particular time, only a single sensor is used to collect the vibration data which requires underdetermined SI (i.e., the number of sensors is less than the number of modal responses). However, the traditional methods are unable to perform SI using single sensor measurement.
- Most of the output-only SI methods require selection of model orders (i.e., time-domain methods) and basis functions (i.e., time-frequency methods) which are time-intensive in nature and involve significant user-intervention, hindering their real-time application in mobile sensing technology.

- EMD is suitable for single sensor measurements. However, EMD has mode-mixing issue that requires special treatment to separate modal responses.
- The vibration measurements of civil engineering systems are contaminated with measurement noise that causes significant inaccuracies in the modal identification.
- Large-scale civil engineering structures exhibit several closely-spaced modes. In order to separate these frequencies, one requires a robust SI method that can identify multiple frequencies in ease.

1.5 Thesis Objectives

With gap areas of existing SI methods as identified above, the main objectives of this thesis are summarized as follows. The proposed method is developed addressing these specific challenges.

- To develop a new output-only time-frequency algorithm for system identification of structures that utilizes only single channel measurement. Once developed, this technique can be directly implemented to mobile sensing network for real-time applications and automation;
- To develop a robust EMD method (e.g., free of any basis functions) that can perform accurate modal identification without causing mode-mixing in the modal responses. The robustness of the method is especially concerned with measurement noise and closely-spaced frequencies such that it can be employed in a wide range of civil structures; and

- To demonstrate and validate the proposed method to several numerical, laboratory and full-scale structures.

The thesis is outlined as follows. First, a background of EMD is presented in **Chapter 2** followed by the formulation of the proposed algorithm. In **Chapter 3**, numerical simulations are conducted using a wide range of dynamical models subjected to various excitations. Experimental and full-scale studies are conducted in **Chapter 4** using a lab-scale model and a pedestrian bridge. Finally, the conclusions of the research are given in **Chapter 5** followed by a list of major contributions and recommendations for future work.

Chapter 2

Proposed Method

In this chapter, time-varying filter-based empirical mode decomposition (TVF-EMD) algorithm is explored as a possible method for modal identification of dynamical systems. The TVF-EMD method is derived from the equation of motion of a dynamical system using the classical theories of structural dynamics. Root-mean-square values of the IMFs are utilized to develop a cluster diagram of the identified frequencies from which key structural frequencies are identified in an automated manner. Unlike EMD, the TVF-EMD method can extract the modal responses using single vibration measurement without any mode mixing issue. A brief background of the EMD and TVF-EMD method is presented first before going into the details of the proposed algorithm. Once developed, the novelty of the proposed method is discussed at the end.

2.1 Background

In this section, a brief background of EMD and TVF-EMD is presented followed by a suite of numerical illustration with the aid of harmonic signals. The effectiveness of the TVF-EMD method is demonstrated using examples of closely-spaced frequencies and measurement noise added to the mixed signals. It will be shown how the TVF-EMD method can be considered as a modal identification method for dynamical system.

2.1.1 Empirical Mode Decomposition

The empirical mode decomposition (EMD) [53] is one of the popular time-frequency domain methods and a powerful data-driven technique that can work with nonlinear and nonstationary signal. The EMD method decomposes the signal into a set of oscillatory waveforms known as intrinsic mode functions (IMFs). An IMF is a function that satisfies the following two conditions [53]:

- In the whole data set, the number of extrema and the number of zero crossings must be either equal or differ by not more than unity.
- At any point, the average of the envelope set by the local maxima and the envelope set by the local minima is zero.

In order to satisfy above criteria, the fundamental steps of EMD to decompose $y(t)$ signal are as follows:

1. Select all the local extrema and prepare a cubic spline line on all of the local minima and local maxima as the lower and upper envelopes. All the data in between have to be covered by the lower and upper envelopes. Their mean is designated as k_1 , and the difference between the data $y(t)$ and k_1 is defined by

$$h_1 = y(t) - k_1 \tag{2.1}$$

If h_1 satisfies the two conditions of IMF that mentioned above, then h_1 should be the first IMF of signal $y(t)$.

2. If h_1 does not satisfy the conditions, presume h_1 as the original data $y(t) = h_1(t)$ and repeat the sifting process with $i_1 = h_1$ until the requirements are met and the first IMF is obtained.

3. The $y(t)$ is then deducted from the IMF and the another IMF is obtained by applying the sifting process again to the remaining signal. The process is iterated to obtain n IMFs, as shown in:

$$y(t) = \sum_{j=1}^n i_j(t) + p_n(t) \quad (2.2)$$

Where $i_j(t)$ ($i = 1, 2, \dots, n$) represents the IMFs of the signal $y(t)$ from higher to lower frequency components, and each $i_j(t)$ contains a different frequency component. $p_n(t)$ is the mean residual trend of the signal or a constant. However, due to multiple averaging process of EMD, this step results in the IMFs that have more than one component of the natural frequency which is known as *mode-mixing* [54]. In order to alleviate mode-mixing, [54] introduced intermittency-based criteria. For example, let us consider a mixed signal of two harmonic waves:

$$y(t) = a_1 \cos(2\pi\omega_1 t) + a_2 \cos(2\pi\omega_2 t) \quad (2.3)$$

A criterion frequency f_{int} (i.e., the intermittency frequency) similar to band-pass filter is applied to eliminate the mode mixing. The f_{int} is defined based on the period length to decompose the signals into different modes [63]. This approach enables extraction of a modal response as mono-component IMF. Thereafter, similar steps are repeated for all IMFs.

Numerical Illustration of EMD

A following mixture of three harmonic signals are decomposed to show the efficiency of the EMD method.

$$s_1 = \sin(2\pi\omega_1 t), \quad s_2 = \sin(2\pi\omega_2 t), \quad s_3 = \sin(2\pi\omega_3 t) \quad (2.4)$$

$$y(t) = s_1 + s_2 + s_3 \quad (2.5)$$

Where $\omega_1 = 5$ Hz, $\omega_2 = 7$ Hz, and $\omega_3 = 10$ Hz. Fig. 2.1 shows original sine signals, their mixed signal and Fourier spectrum. It can be seen that there are three harmonic frequencies that are clearly visible in Fourier spectrum. The estimated frequency limit between higher and lower frequency for each individual natural frequency, i.e., $\omega_{hj} > \omega_j > \omega_{lj}$, can then be extracted from the Fourier spectrum.

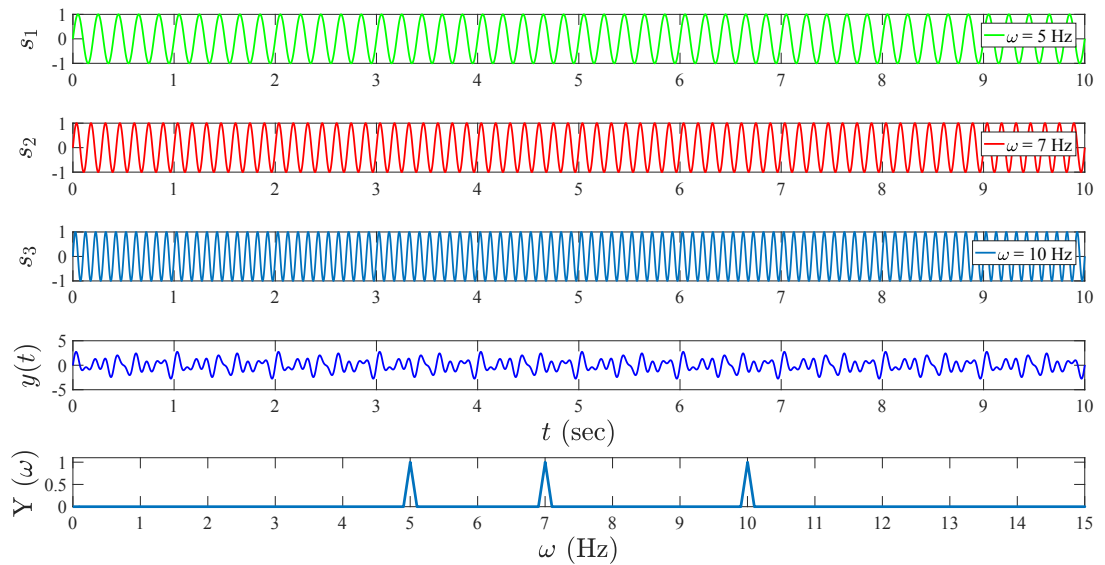


Figure 2.1: Original sine signals, their mixed signal and Fourier spectrum

First, the EMD method is applied to the mixed signal $y(t)$ with the upper and lower intermittency frequency bands. The first IMF and its Fourier transform are shown in the first column of Fig. 2.2. It can be seen that i_1 has the mono-component frequency (one peak) which is the first sine frequency of the signal $y(t)$. To extract the next harmonic signal, EMD is applied to the rest signal without considering ω_1 . The second column of Fig. 2.2 shows the resulting IMF and its Fourier transform. Again, only there is one peak in the spectrum which is the second sine frequency of the signal $y(t)$. The procedure is repeated, and the last frequency is obtained from the EMD as shown in the third column of Fig. 2.2.

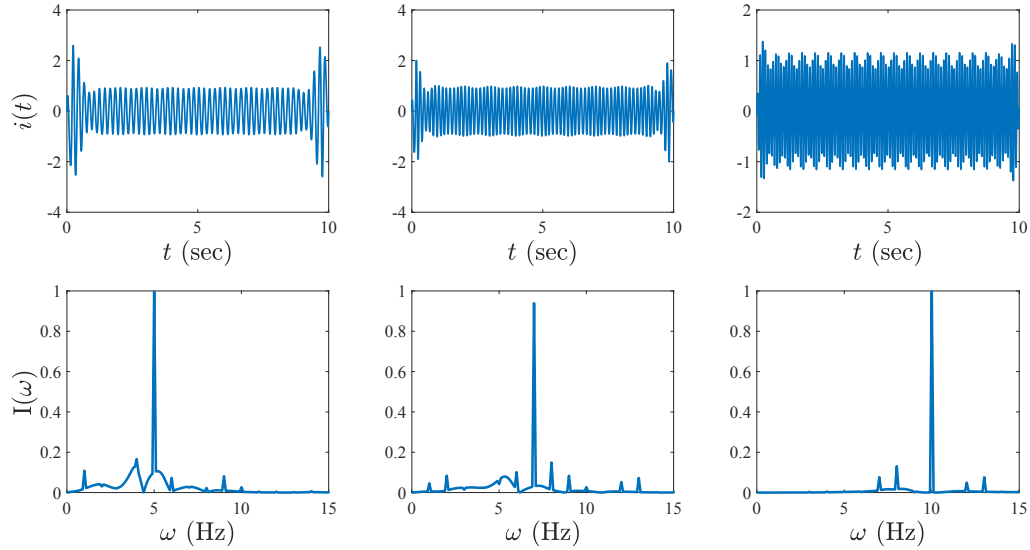


Figure 2.2: IMFs of $y(t)$ and its Fourier spectrum

As shown above, the EMD method has an attractive feature of extracting hidden signal components from their mixed signal. However, the EMD method has several limitations as follows:

- Mode-mixing of the EMD can be eliminated using intermittency criteria, however such an approach is subjective and requires significant user intervention.
- The EMD is sensitive to noise and is computationally intensive for dynamical systems with higher degrees-of-freedom (e.g., flexible civil structures).
- As shown in Fig. 2.2, EMD has significant end-effect that causes hindrance to accurately calculating damping calculations for structural systems.

2.1.2 Time-Varying Filtering-based EMD

In traditional EMD method, the estimation of the local mean can be observed as a unique form of low pass filtering [76]. In time-varying filter-based EMD method

(TVF-EMD), a B-spline approximation is adopted as a criteria to select time-varying filter. Most of the present works use B-splines as an interpolation tool with polynomial spline. However, TVF-EMD use B-spline functions which are piecewise polynomials with time-varying cut-off frequencies. With such property, the TVF-EMD can deal with single vibration measurement to identify all frequencies without any mode-mixing issue in the modal responses. In order to form the desired signal, the polynomial portions are joined together. The joining points of the polynomial sections are denoted as knots. Every signal in B-spline space can be determined by [55]:

$$g_m^n(t) = \sum_{j=-\infty}^{+\infty} r(j)\beta^n(t/m - j) \quad (2.6)$$

Where $r(j)$ is the B-spline coefficients and it is enlarged by a factor of m . The signal (or approximation result) is determined by n, m , and $r(j)$. That means, given the B-spline order and knots, the B-spline approximation is used to determine the B-spline coefficients $r(j)$ that minimizes the approximation error. Let $b_m^n(t) = \beta^n(t/m)$ and the asterisk denotes the convolution operator, For an original signal $y(t)$, $r(j)$ is determined by minimizing the approximation error ε_m^2 :

$$\varepsilon_m^2 = \sum_{t=-\infty}^{+\infty} (y(t) - [r]_{\uparrow m} * b_m^n(t))^2 \quad (2.7)$$

Where $[\cdot]_{\uparrow m}$ is the up-sampling operation (adding zeros between each sample) by m . After introducing the concept of B-spline approximation (i.e., revealing its low-pass filtering property), the solution of $r(j)$ is

$$r(j) = [l_m^n * y]_{\downarrow m}(r) \quad (2.8)$$

Where $[\cdot]_{\downarrow m}$ is the down-sampling operation by m and l_m^n is the pre-filter denoted by

$$l_m^n = [([b_m^n * b_m^n]_{\downarrow m})^{-1}]_{\uparrow m} * b_m^n \quad (2.9)$$

We can now rewrite $g_m^n(t)$ Eq. 2.6 as:

$$g_m^n(t) = [l_m^n * y]_{\downarrow m} * b_m^n(t) \quad (2.10)$$

By observing the equations, there are three steps to carry out the B-spline approximation of a signal. The signal y is first band-limited through a pre-filter b_m^n . Next, by a factor of m , the band-limited signal is decimated. Finally, the approximation is reconstructed using a post-filter b_m^n .

Numerical Illustration of TVF-EMD

In this section, TVF-EMD method is illustrated using two different examples with varying level of measurement noise.

- Example 1: Same example as shown in Eq. 2.5 with 0%, 5% and 10% measurement noise, respectively.
- Example 2: Frequencies of three harmonic signals of Example 1 are chosen differently to simulate closely-spaced frequencies. The frequencies are selected as 5 Hz, 5.5 hz and 6 Hz, respectively.

(a) Example 1

In this example, three signals are assumed as mentioned in Eq. 2.4 and 2.5, where $\omega_1 = 5$ Hz, $\omega_2 = 7$ Hz, and $\omega_3 = 10$ Hz, respectively. Fig. 2.3 shows original sine signals and their mixed signal with 0% measurement noise. Fig. 2.4 shows the IMFs and its Fourier transform by using the TVF-EMD method. It can be observed that the TVF-EMD method has extracted the mono-component components of the original signal $y(t)$ successfully without applying intermittency criteria. Moreover,

unlike EMD, the TVF-EMD does not result in end-effects (compared with Fig. 2.2) and shows clear signal separations.

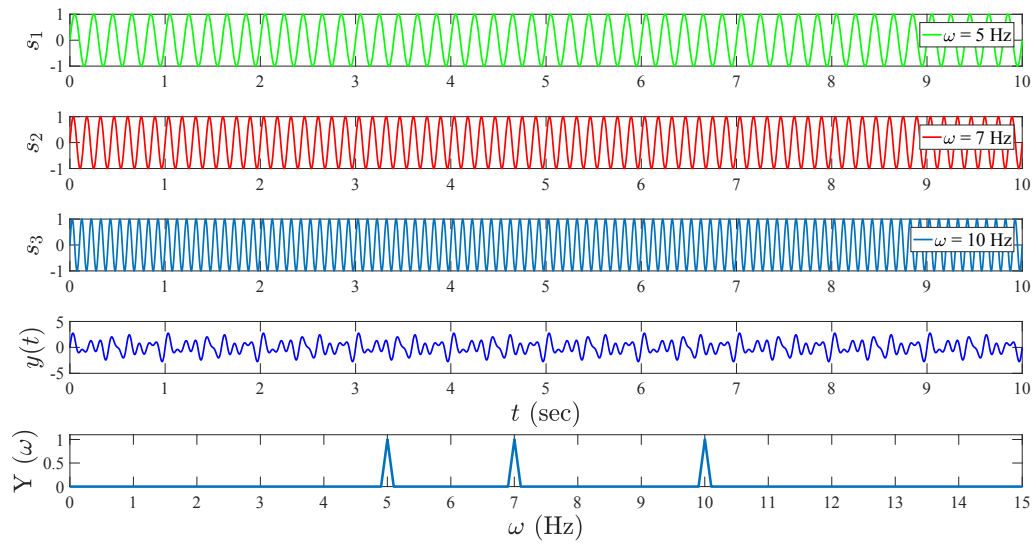


Figure 2.3: Original sine signals, their mixed signal and Fourier spectrum under 0% noise

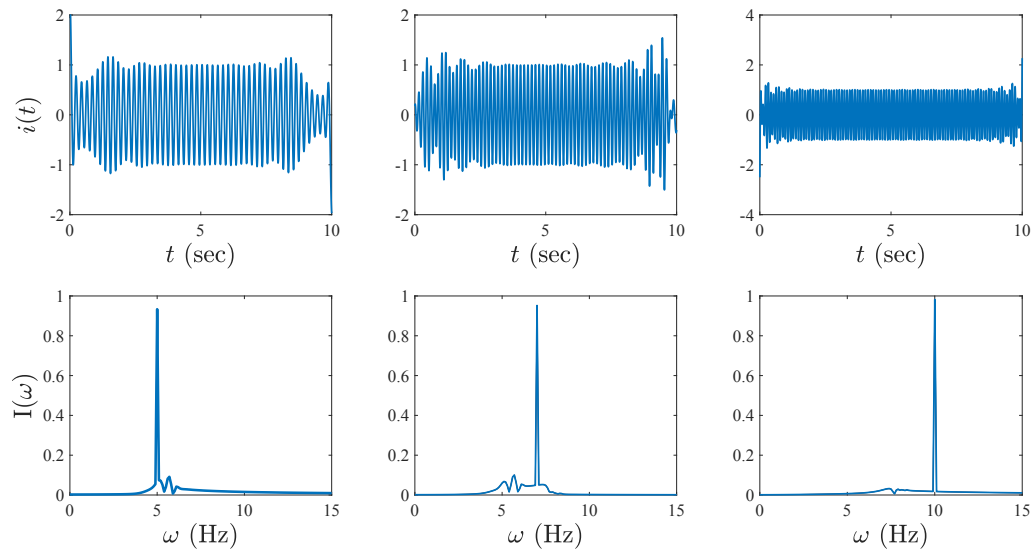


Figure 2.4: The IMFs and its Fourier spectrum under 0% noise

Fig. 2.5 and Fig. 2.7 show the original time data and corresponding Fourier spectrum of the mixed signal with 5% and 10% measurement noise, respectively. Fig. 2.6 and 2.8 show the resulting IMFs and its Fourier transform obtained from the TVF-EMD method. It can be observed that the TVF-EMD method has extracted the mono-component IMFs of each original signal $y(t)$ successfully even with 5% and 10% measurement noise without any end effects.

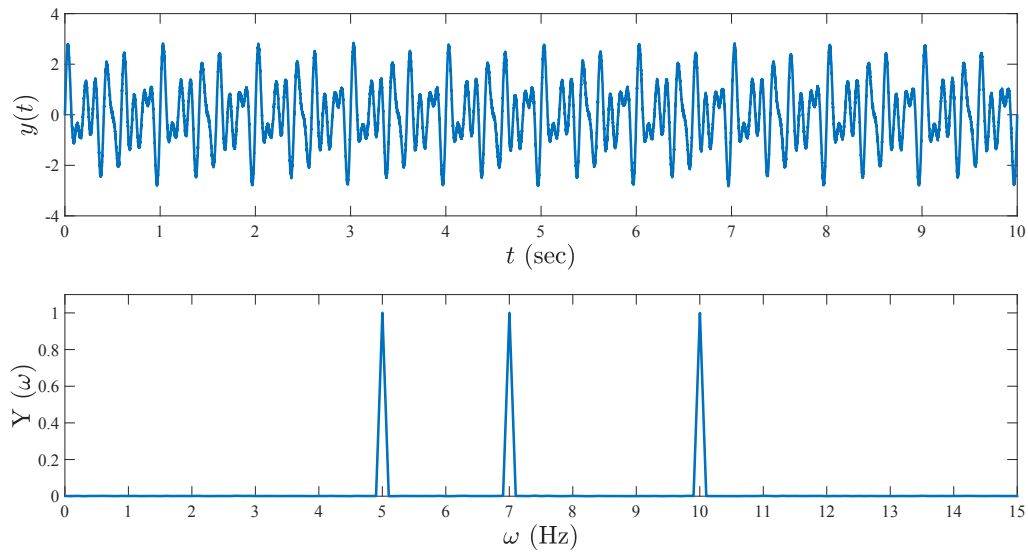


Figure 2.5: Mixed signal and its corresponding Fourier spectrum under 5% noise

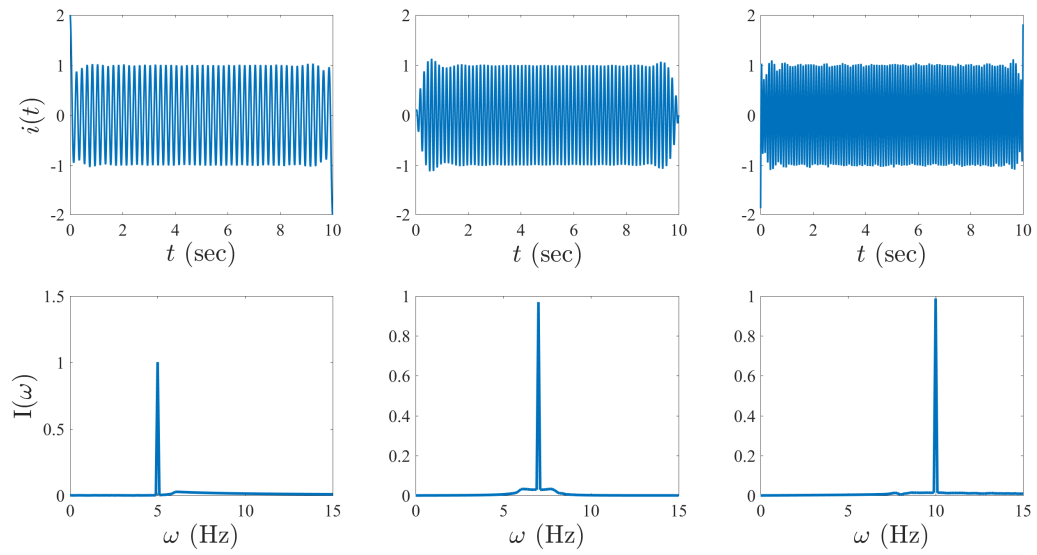


Figure 2.6: The IMFs and its Fourier spectrum under 5% noise

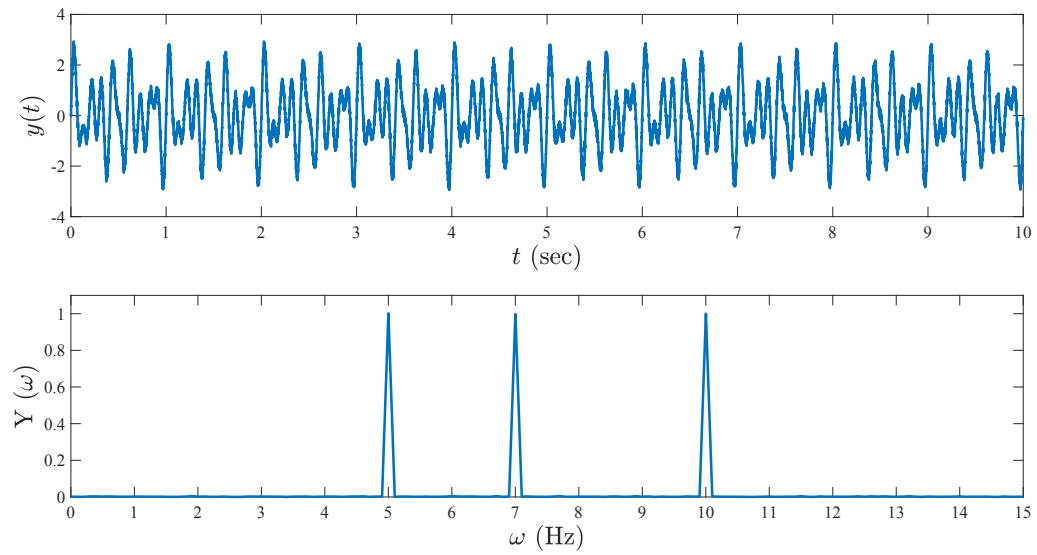


Figure 2.7: Mixed signal and its corresponding Fourier spectrum under 10% noise

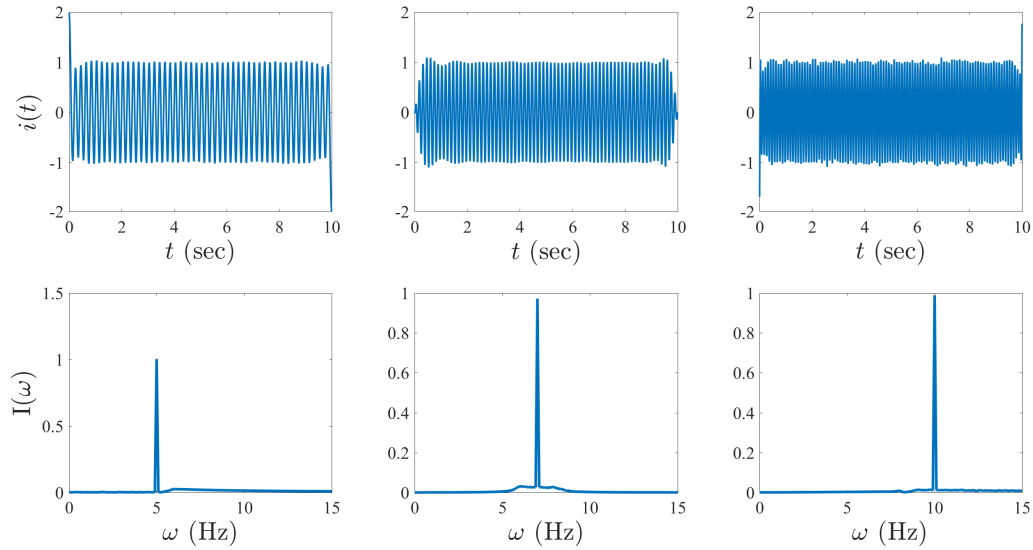


Figure 2.8: The IMFs and its Fourier spectrum under 10% noise

(b) Example 2

In order to check the efficiency of TVF-EMD method under closely-spaced frequencies, a mixture of three sine signals is considered with frequencies 5, 5.5 and 6 Hz, respectively. Fig. 2.9 shows the original time data and corresponding Fourier spectrum of the data with 5% noise. Fig. 2.10 shows the IMFs and its Fourier transform by using the TVF-EMD method with 5% noise. Similar exercise is repeated with the mixed signal contaminated with 10% measurement noise and the results are shown in Fig. 2.11 and 2.12, respectively. It can be seen that the TVF-EMD method has successfully identified the mono-component modal response of each signal under 5% and 10% measurement noise even under closely-spaced frequencies as shown in Fig. 2.10 and Fig. 2.12, respectively.

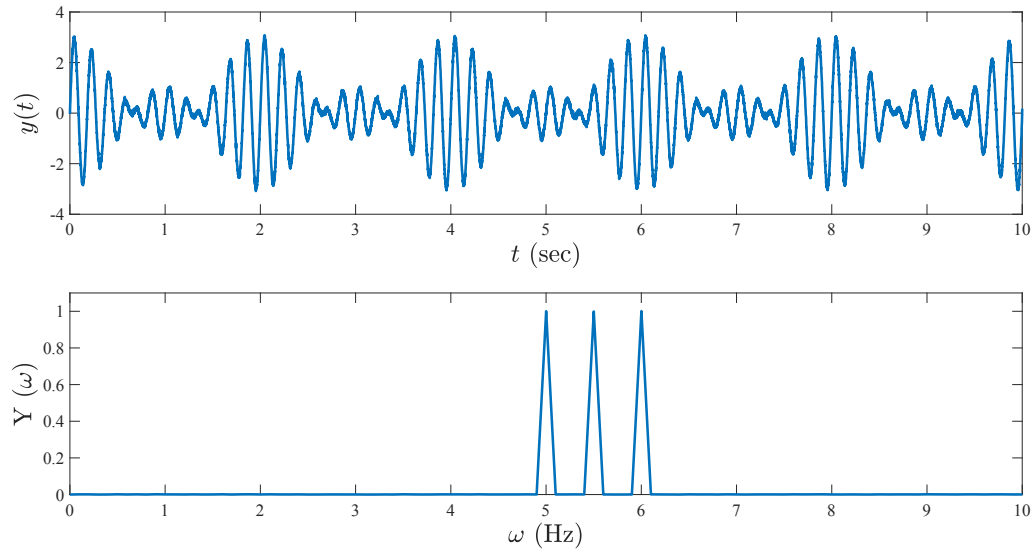


Figure 2.9: Mixed signal and its corresponding Fourier spectrum under 5% noise

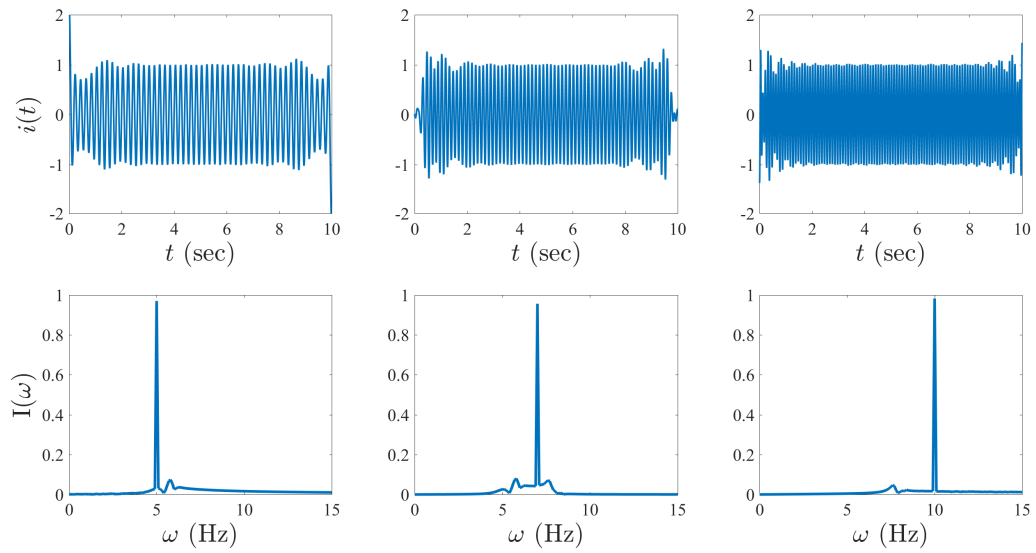


Figure 2.10: The IMFs and its Fourier spectrum under 5% noise

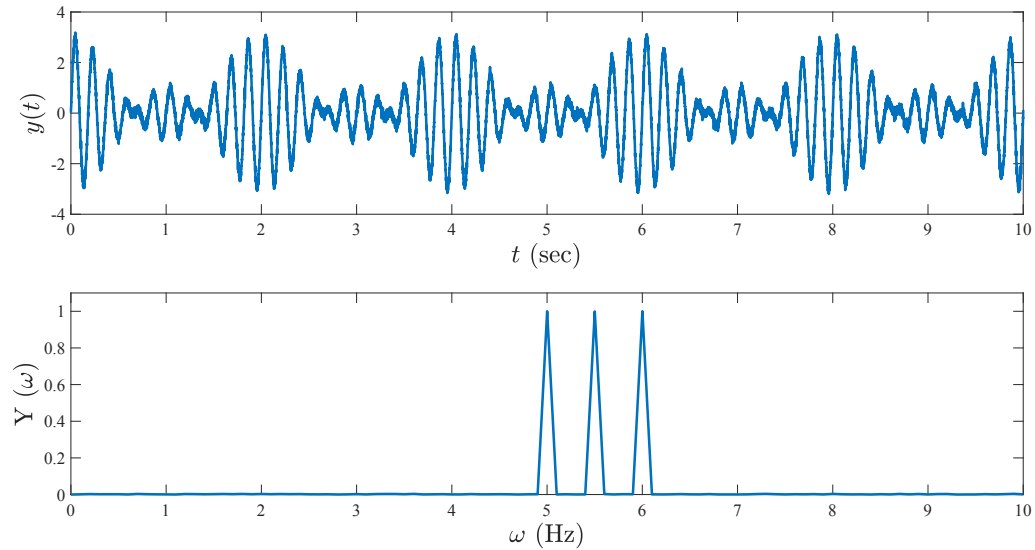


Figure 2.11: Time domain data and corresponding Fourier spectrum

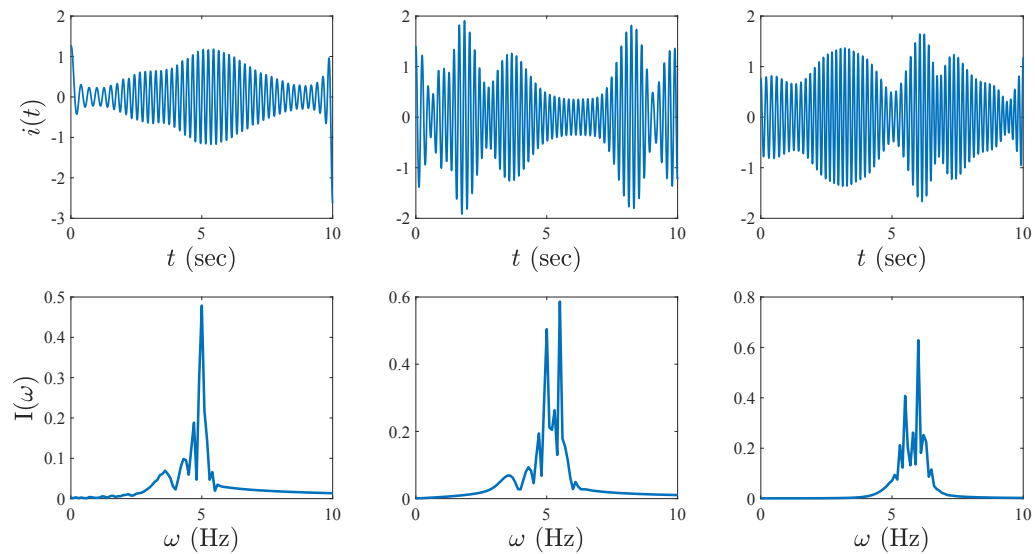


Figure 2.12: The IMFs and its Fourier spectrum under 10% noise

2.2 Proposed Methodology

With a brief background of the TVF-EMD method, let us now formulate the proposed method from the equation of motion of a dynamical system. Consider a linear,

classically damped and lumped-mass n degrees-of-freedom (DOF) structural system, subjected to a wide-band random input force, $\mathbf{u}(t)$:

$$\mathbf{M}\ddot{\mathbf{x}}(t) + \mathbf{C}\dot{\mathbf{x}}(t) + \mathbf{K}\mathbf{x}(t) = \mathbf{u}(t) \quad (2.11)$$

where, $\mathbf{x}(t)$ is a vector of displacement response at DOFs. \mathbf{M} , \mathbf{C} and \mathbf{K} are mass, damping and stiffness matrices, respectively. The solution to Eq. 2.11 for any dynamical system can be formulated using the state-space model with following form:

$$\bar{\mathbf{x}} = \begin{bmatrix} \mathbf{x}_1 \\ \mathbf{x}_2 \end{bmatrix} \quad (2.12)$$

$$\dot{\bar{\mathbf{x}}} = \mathbf{A}\bar{\mathbf{x}} + \mathbf{B}\mathbf{u} \quad (2.13)$$

$$\mathbf{y} = \mathbf{C}\bar{\mathbf{x}} + \mathbf{D}\mathbf{u} \quad (2.14)$$

where \mathbf{A} is the state matrix, \mathbf{B} is input matrix, \mathbf{C} is the output matrix, and \mathbf{D} is transmission matrix. Under broad-band excitation $\mathbf{u}(t)$, the resulting solution of Eq. 2.11 can be written in terms of an expansion of vibration modes:

$$\mathbf{x} = \Phi\mathbf{q} \quad (2.15)$$

where, \mathbf{x} and \mathbf{q} is the response and modal coordinate matrix, respectively. $\Phi_{m \times n}$ is the modal transformation matrix. n and m is the number of modal responses and measurements, respectively. The measurement at the k -th DOF ($k = 1, 2, \dots, m$) of Eq. 2.15 can be expressed as

$$x_k(t) = \sum_{j=1}^n \phi_{kj} q_j(t) \quad (2.16)$$

Performing TVF-EMD of $\mathbf{x}(\mathbf{t})$, we can express each signal of $\mathbf{x}(\mathbf{t})$ in terms of its IMFs (i.e., i_{kj}):

$$x_k(t) = \sum_{j=1}^n i_{kj}(t) \quad (2.17)$$

Comparing Eq. 2.17 and Eq. 2.16, we get:

$$\phi_{kj}q_j(t) = i_{kj}(t) \quad (2.18)$$

$$q_j(t) = ci_{kj}(t) \quad (2.19)$$

where c is a constant multiplier. Eq. 2.19 also states that modal responses can be extracted using the IMFs. However, TVF-EMD results in a finite number of IMFs. In order to select dominant IMFs that contain modal responses, a root-mean-square (RMS) based thresholding criteria is set up. It is proposed that the IMFs that have RMS values higher than mean RMS value of all IMFs (μ_{rms}) are considered for estimation of frequencies. The resulting scatter diagram of the frequencies are used to select the specific IMF that includes modal responses. Once the modal response is identified, autocorrelation function of IMF is used to estimate the modal damping. The proposed method is illustrated using the flowchart as shown in Fig. 2.13.

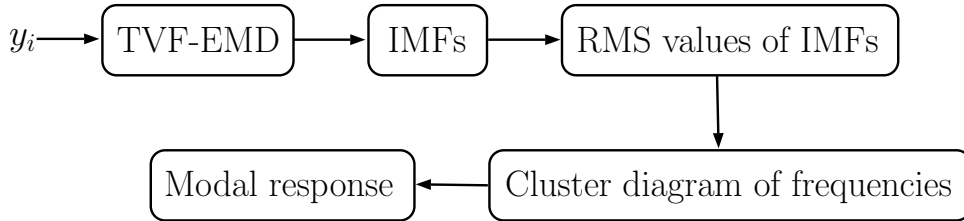


Figure 2.13: Flowchart of the proposed method

Chapter 3

Numerical Study

In this chapter, the proposed method is validated using three different numerical models (namely, the 3-DOF, 4-DOF and 10-DOF models) to perform modal identification using single sensor measurement in a decentralized mobile sensing framework. The properties of these models are chosen such that they cover a wide range of dynamical characteristics including closely spaced frequencies and low energy modes. The mass and stiffness of these models are appropriately selected to reflect realistic dynamic behaviour of flexible civil engineering systems.

3.1 3-DOF Model

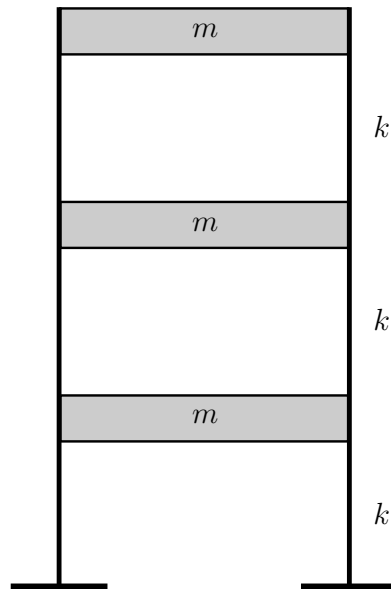


Figure 3.1: 3-DOF model

A 3-DOF discrete lumped mass dynamical system is considered as shown in Fig. 3.1. The lumped mass and stiffness are assumed to be 144 tonne, and 2×10^8 N/m, respectively in each floor. A modal damping of 5% is assumed for first two modes with Rayleigh damping approximation. The resulting natural frequencies are 2.65, 7.44 and 10.75 Hz, respectively. The model is then excited by Imperial Valley earthquake at its base. The time-history and Fourier spectrum of the ground motion is shown in Fig. 3.2. Fig. 3.3 shows the Fourier spectra of floor vibration measurements. As shown in Fig. 3.2, the earthquake has significant energy only within 7.5 Hz. Such excitation excites only first two modes of the 3-DOF model that appear in the Fourier spectra of response in Fig. 3.3. Therefore, the number of target modes is selected as 2 (i.e., first two modes).

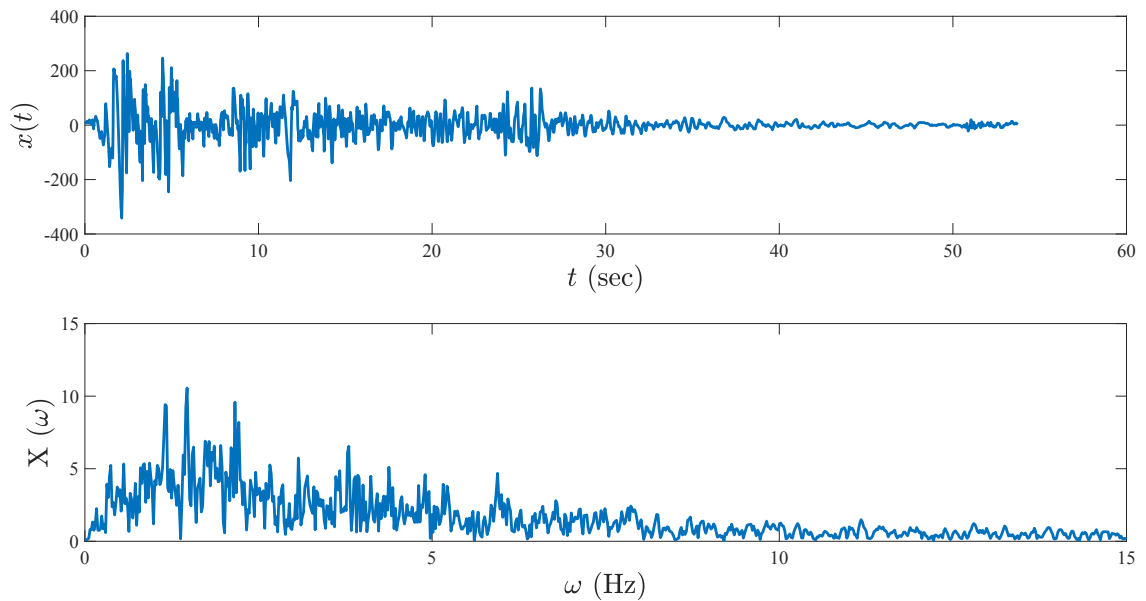


Figure 3.2: Time-history and Fourier spectra of the ground motion

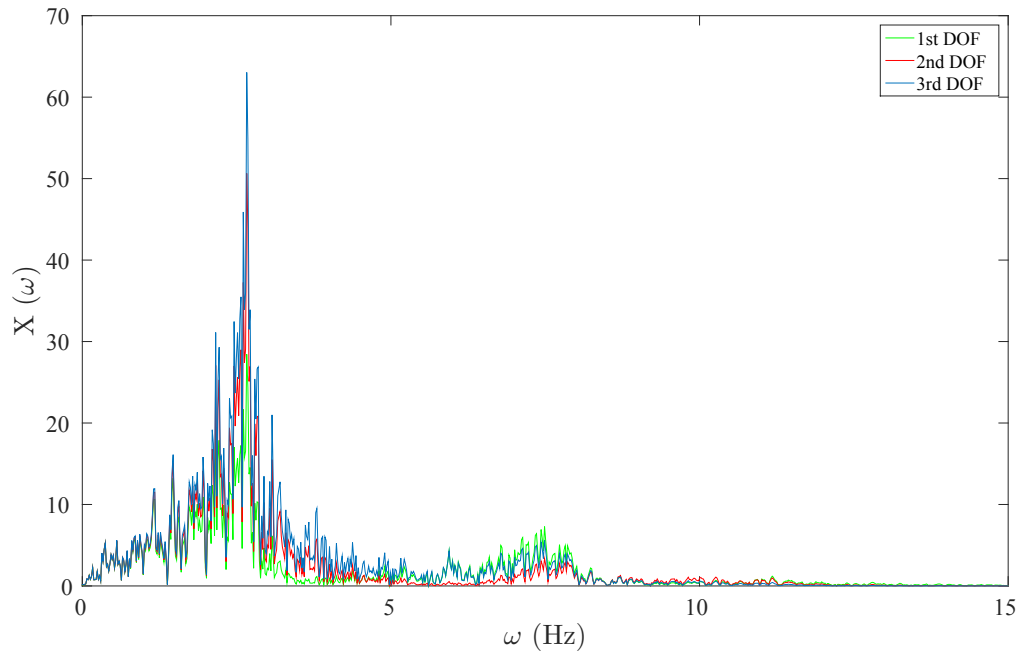


Figure 3.3: Time-history and Fourier spectra of floor responses

The TVF-EMD method is applied on each floor measurement separately. When the first floor measurement is chosen, it results in 155 IMFs. The RMS value of each IMF is calculated and plotted in Fig. 3.4 to identify dominant frequency components of the measurement that have RMS values higher than the average RMS value of all IMFs (as highlighted in red line). Fig. 3.5(a) and (b) show the cluster of frequencies of all IMFs and the IMFs that are above the mean RMS value (i.e., μ_{rms}), respectively. It is observed that the clusters of frequencies that have nearly zero slope coincide with true value of natural frequencies as highlighted in red lines. As stated earlier, the third mode has extremely low energy and is not identified through the proposed method. The resulting IMF components (i.e., extracted modal responses) of these clusters are shown in Fig. 3.6 revealing the efficiency of the proposed method. It can be seen that all IMFs are mono-component signals.

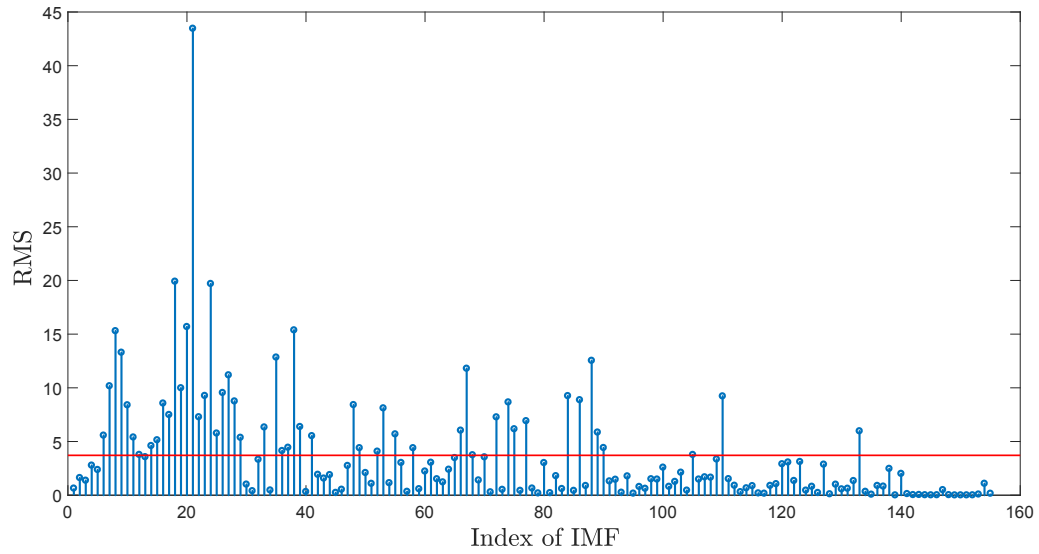


Figure 3.4: RMS values of IMFs of the first floor measurement

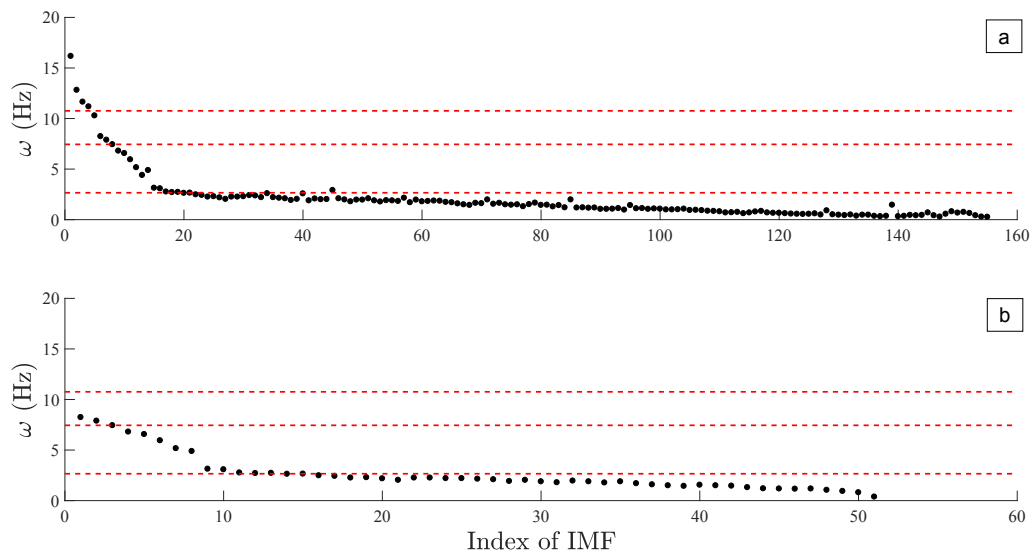


Figure 3.5: Cluster of frequencies of (a) all IMFs and (b) IMFs that are above μ_{rms} in the first floor measurement

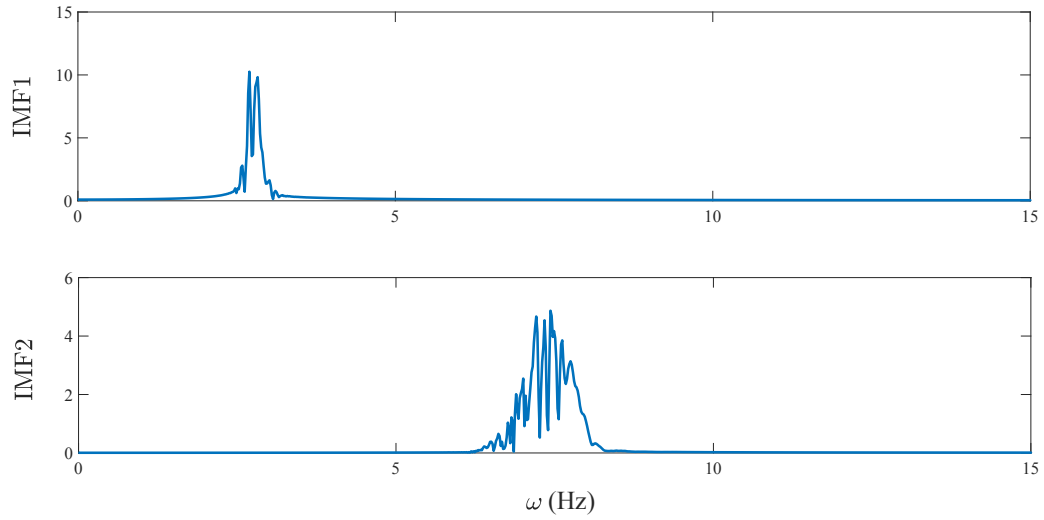


Figure 3.6: IMFs of the first floor measurement obtained from the TVF-EMD method

While using the second floor measurements, the TVF-EMD method has extracted 164 IMFs with RMS values as shown in Fig. 3.7. Fig. 3.8(a) and (b) show the cluster of frequencies of all IMFs and the IMFs that are above the mean RMS value, respectively. Fig. 3.9 shows the IMFs obtained from the second-floor vibration measurements.

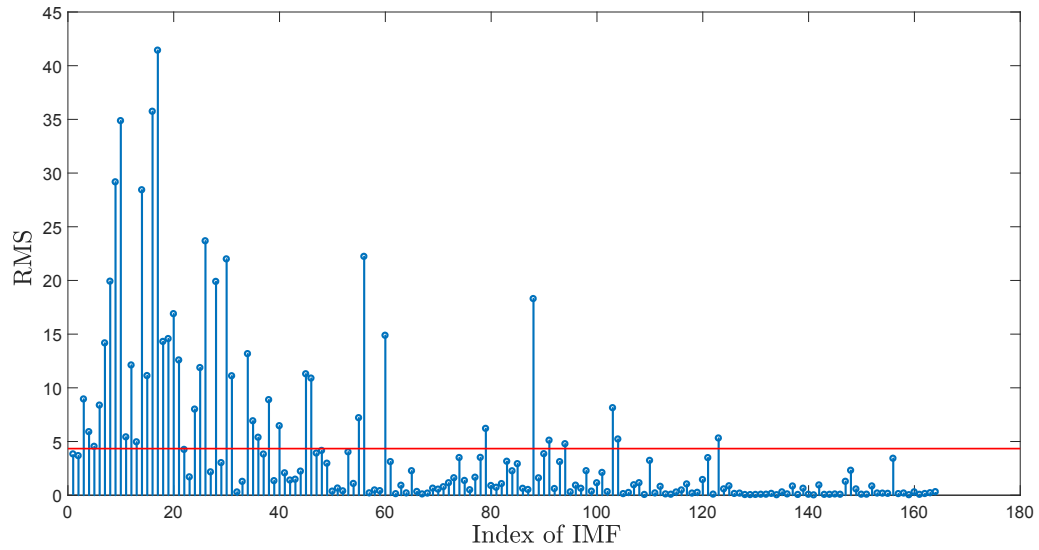


Figure 3.7: RMS values of IMFs of the second floor measurement

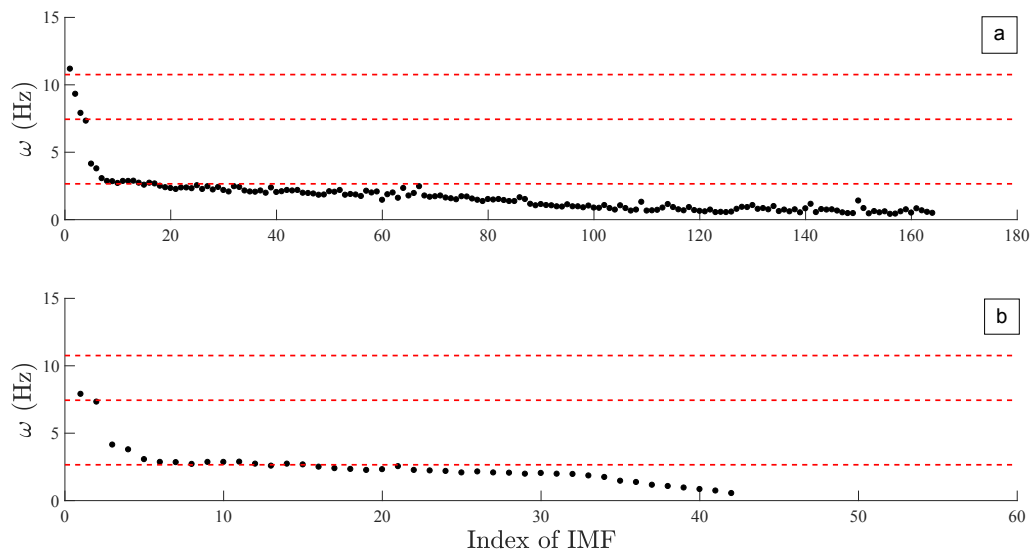


Figure 3.8: Cluster of frequencies of (a) all IMFs and (b) IMFs that are above μ_{rms} in the second floor measurement

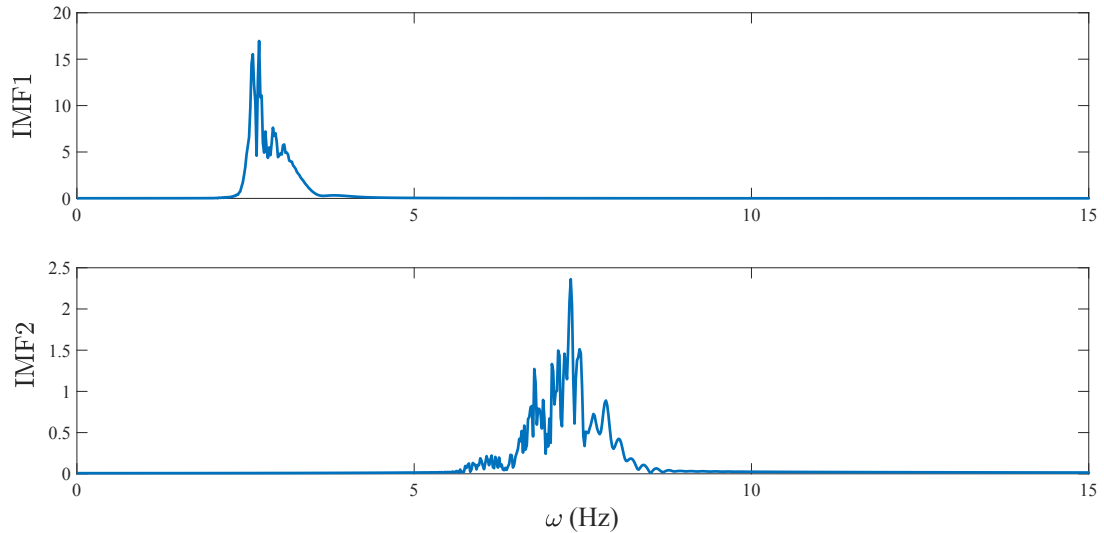


Figure 3.9: IMFs of the second floor measurement obtained from the TVF-EMD

Taking the similar steps, the TVF-EMD method is applied on the third-floor vibration measurements alone and 180 IMFs are obtained from the proposed method as shown in Fig. 3.10. Based on the cluster diagram of frequencies in Fig. 3.11(a) and (b), the modal responses are identified in Fig. 3.12. Once the modal responses are obtained, auto-correlation function of modal responses is used to extract modal damping ratio as shown in Fig. 3.13. Table 3.1 shows comparison of theoretical (ω_i) and identified ($\hat{\omega}_i$) results which reveal significant accuracy of the proposed method.

Table 3.1: Theoretical and identified modal parameters of the 3-DOF model

Mode #	1	2
ω_i (Hz)	2.66	7.45
$\hat{\omega}_1^{(1)}$ (Hz)	2.7	7.44
$\hat{\omega}_2^{(2)}$ (Hz)	2.7	7.32
$\hat{\omega}_3^{(3)}$ (Hz)	2.65	7.49
$\hat{\zeta}_i$ (%)	8.3	6.7

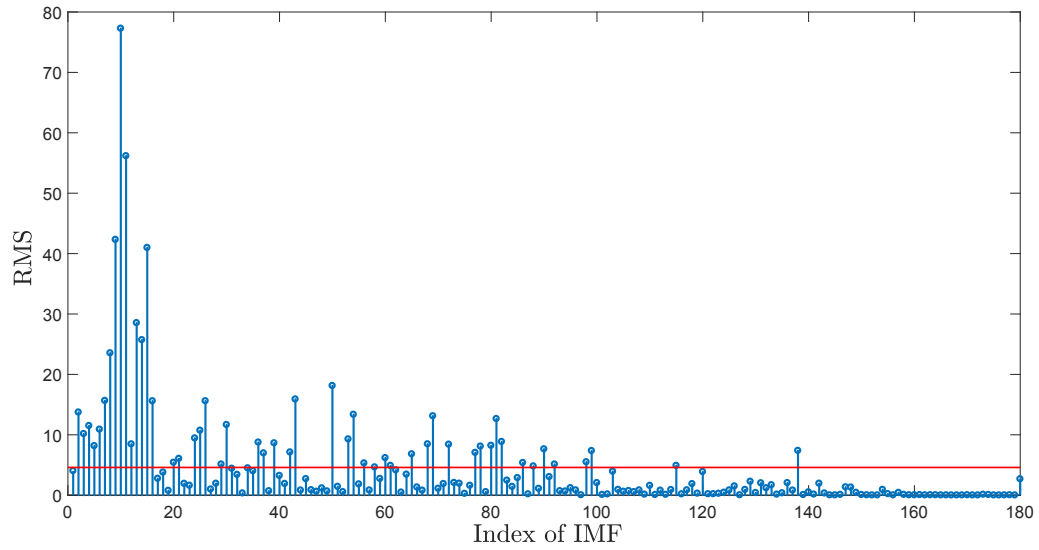


Figure 3.10: RMS values of IMFs of the third floor measurement

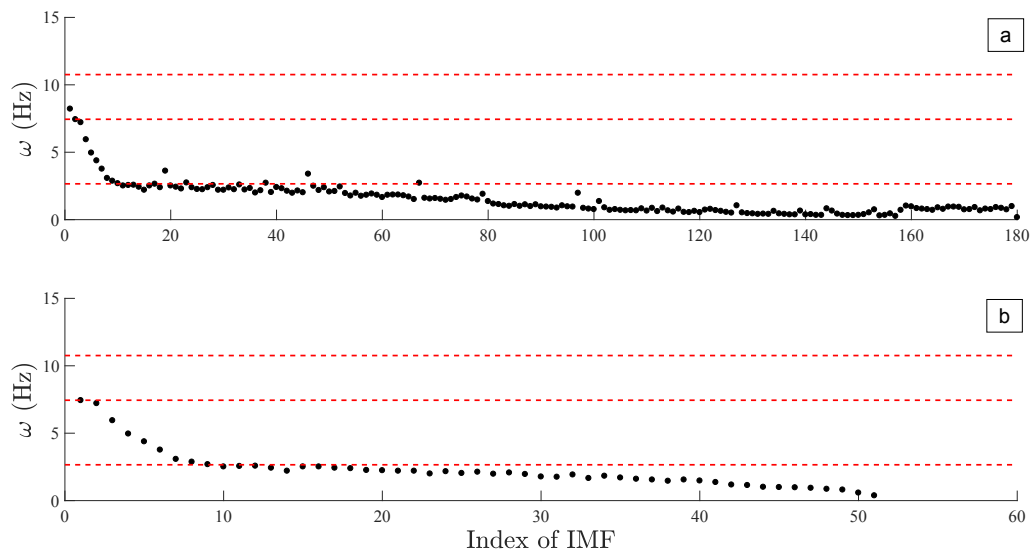


Figure 3.11: Cluster of frequencies of (a) all IMFs and (b) IMFs that are above μ_{rms} in the third floor measurement

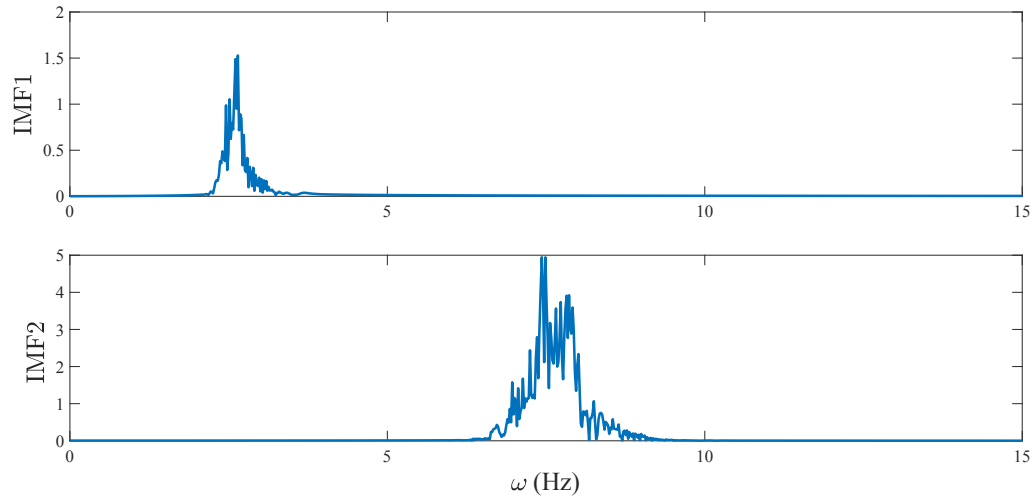


Figure 3.12: IMFs of the third floor measurement obtained from the TVF-EMD

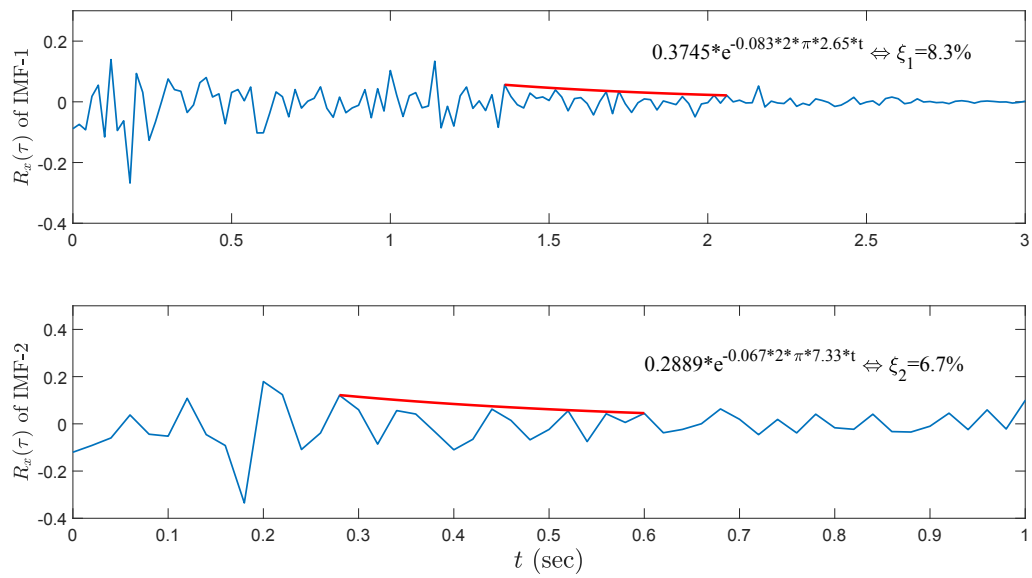


Figure 3.13: Damping ratio of the resulting modal responses of second floor measurement

3.2 4-DOF Model

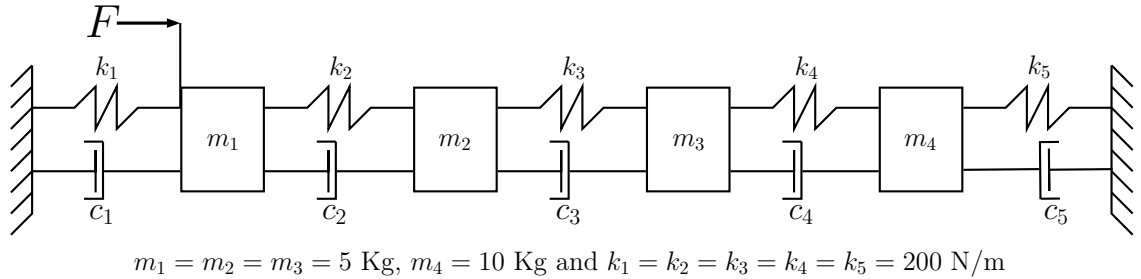


Figure 3.14: 4-DOF model

A 4-DOF dynamical model is now considered with the assumed values of mass and stiffness as shown in Fig. 3.14. A modal damping of 5% is assumed for first two structural modes. The resulting natural frequencies are 0.67, 1.14, 1.53 and 1.88 Hz, respectively. The model is excited by a random force F (with zero mean and unit standard variance) and the resulting vibration measurements are simulated using state-space modeling of the system. Fig. 3.15 shows resulting Fourier spectra

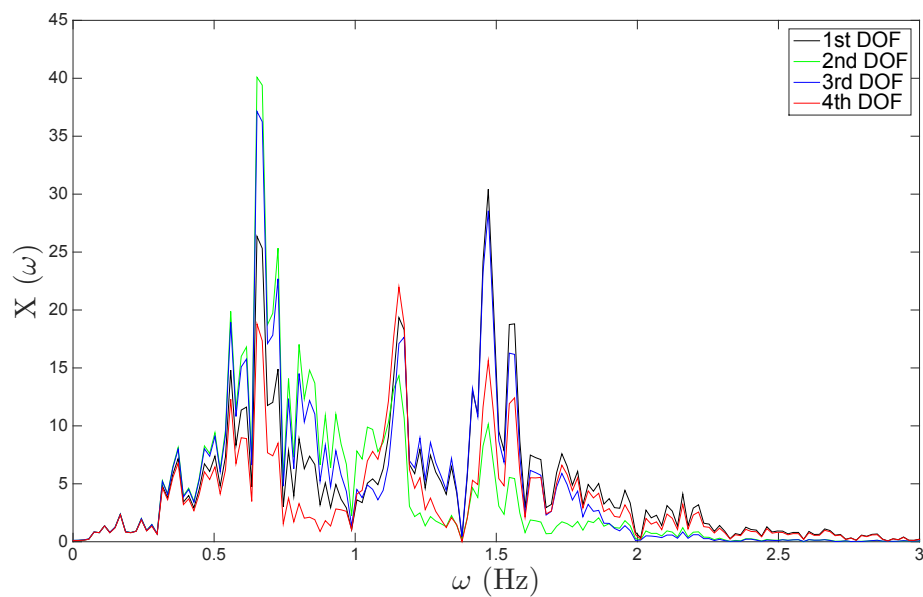


Figure 3.15: Fourier spectra of floor vibration measurements

of vibration measurements at each DOF. The TVF-EMD method is applied on each measurement separately. The vibration measurement of first DOF results in 103 IMFs whose RMS values are shown in Fig. 3.16. Fig. 3.17 (a) shows the cluster of frequencies of all IMFs, whereas Fig. 3.17 (b) shows cluster of frequencies of IMFs that are above the mean RMS values of all IMFs. In Fig. 3.17 (b), it is quite clear that the identified frequencies can be determined where there is zero slope in the cluster diagram of frequencies. Fig. 3.18 shows the typical IMFs obtained from the vibration measurements at first DOF by using the TVF-EMD method.

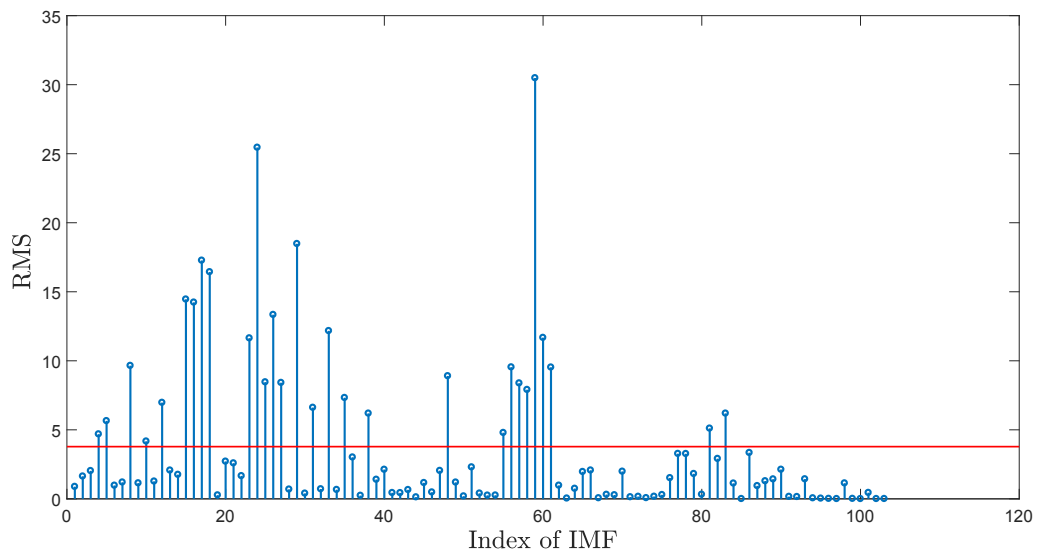


Figure 3.16: RMS values of IMFs of measurement at first DOF

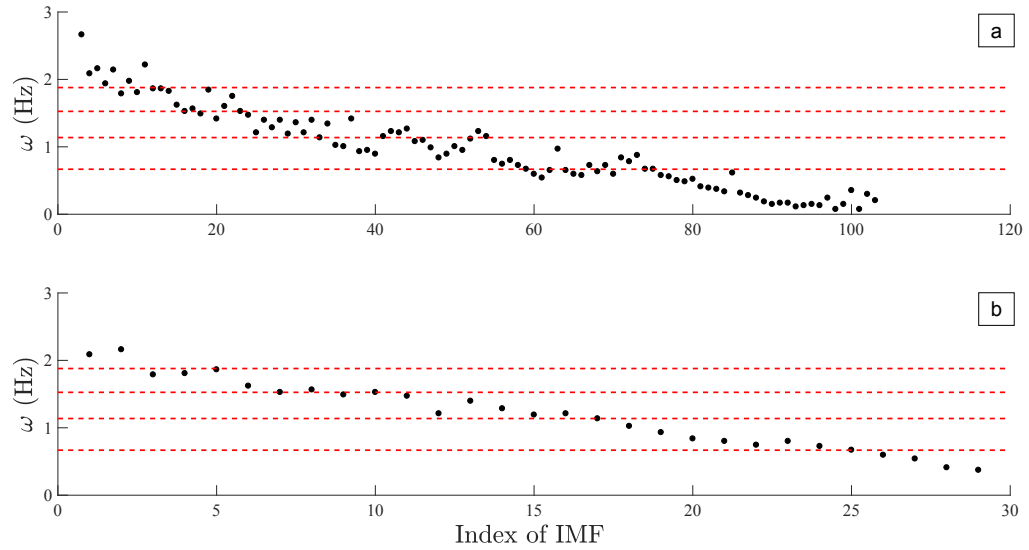


Figure 3.17: Cluster of frequencies of (a) all IMFs and (b) IMFs that are above μ_{rms} in the measurement at first DOF

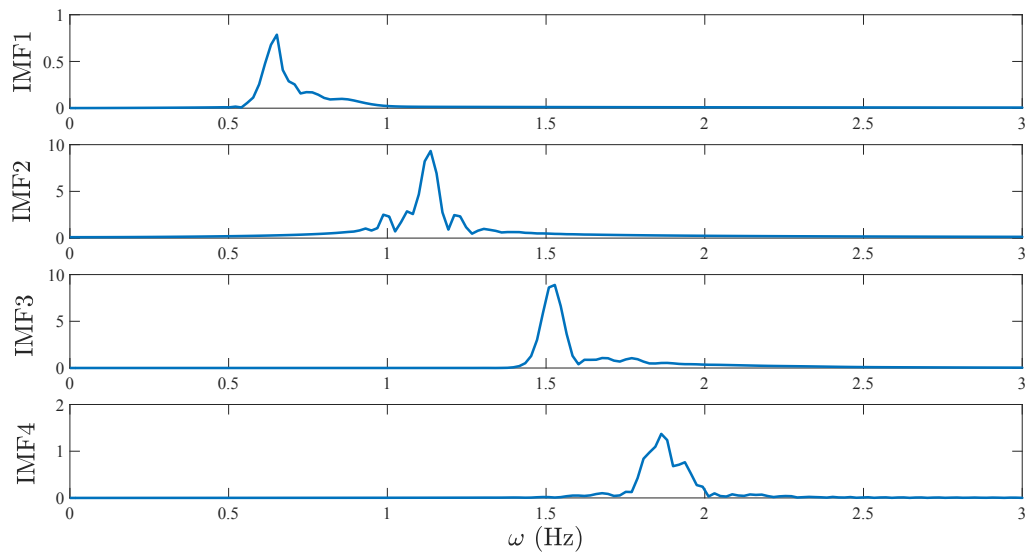


Figure 3.18: IMFs of the measurement at first DOF obtained from the TVF-EMD method

Along the similar process, the measurement at fourth DOF is considered that results in 98 IMFs whose RMS values are shown in Fig. 3.19. Fig. 3.20(a) shows the scatter diagram of all IMFs' frequencies and Fig. 3.20(b) shows the cluster frequencies of IMFs that have relative higher RMS values. Fig. 3.21 shows the resulting modal responses obtained from TVF-EMD method using fourth floor vibration measurement. From these results, it can be observed that the actual frequencies can be easily determined from the cluster diagram of the frequencies that have zero slope. The proposed method has successfully identified all frequencies by using single channel measurement. Once the modal responses are obtained, the auto-correlation function of modal responses is used to extract modal damping ratio. Fig. 3.22 shows the estimation of damping ratio as obtained from the IMFs of vibration measurement of fourth DOF. Table 3.2 summarizes theoretical and identified results of modal identification of the 4-DOF model.

Table 3.2: Theoretical and identified modal parameters of the 4-DOF model

Mode #	1	2	3	4
ω_i (Hz)	0.67	1.14	1.53	1.88
$\hat{\omega}_i^{(1)}$ (Hz)	0.65	1.14	1.53	1.86
$\hat{\omega}_i^{(2)}$ (Hz)	0.72	1.12	1.53	1.92
$\hat{\omega}_i^{(3)}$ (Hz)	0.67	1.15	1.57	1.83
$\hat{\omega}_i^{(4)}$ (Hz)	0.67	1.15	1.47	1.9
$\hat{\zeta}_i$ (%)	4.9	1.2	5	6.6

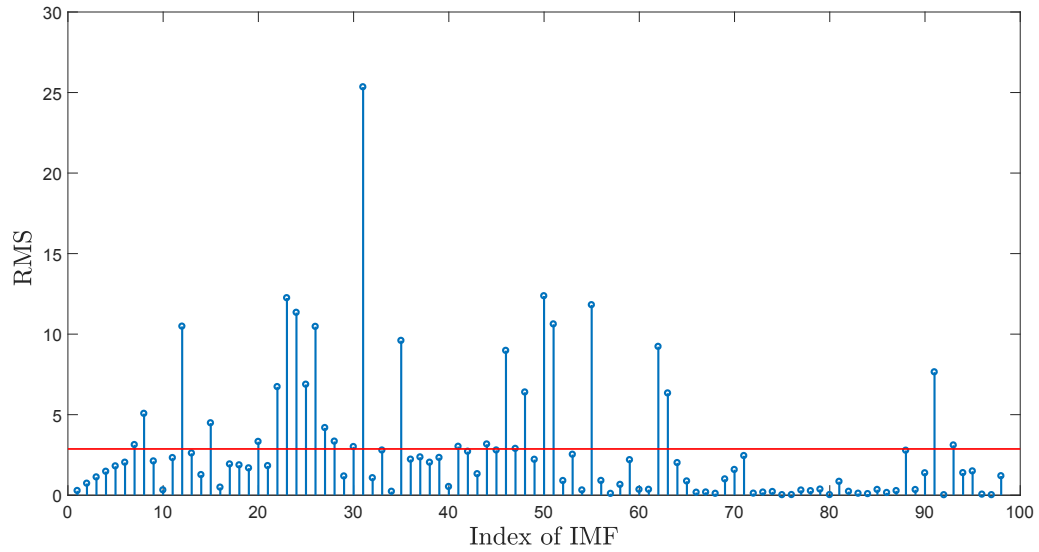


Figure 3.19: RMS values of IMFs of the measurement at fourth DOF

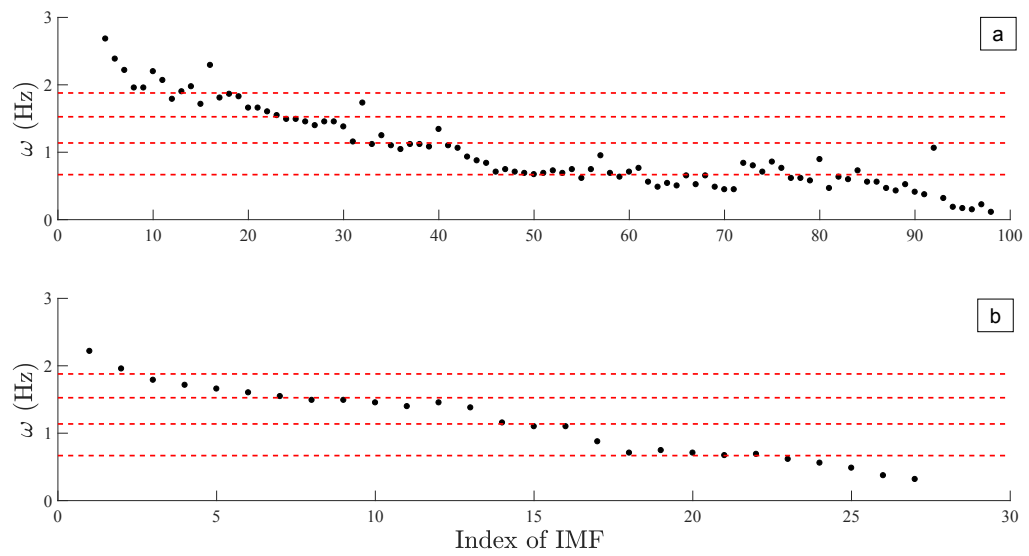


Figure 3.20: Cluster of frequencies of (a) all IMFs and (b) IMFs that are above μ_{rms} in the measurement at fourth DOF

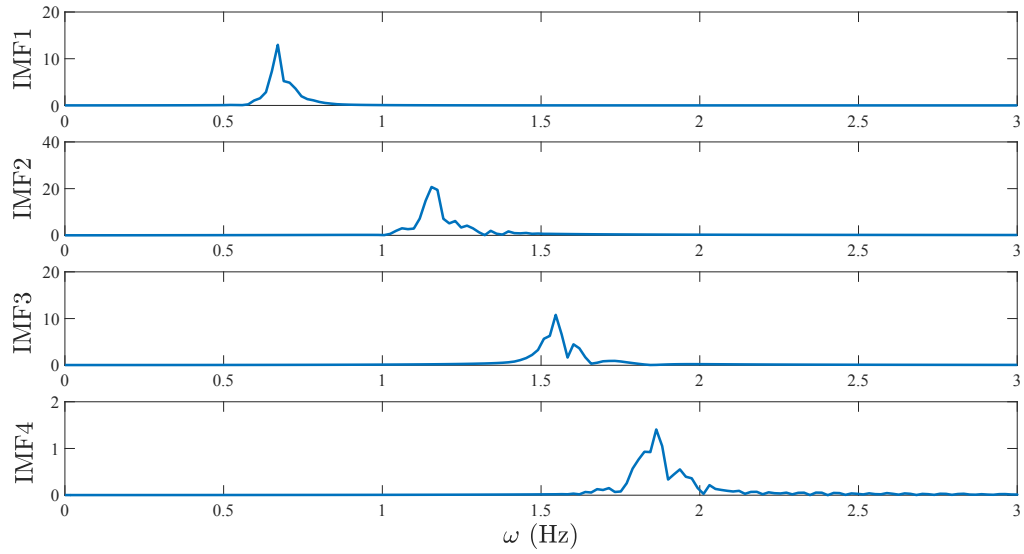


Figure 3.21: Fourier spectra of IMFs of the fourth floor measurement

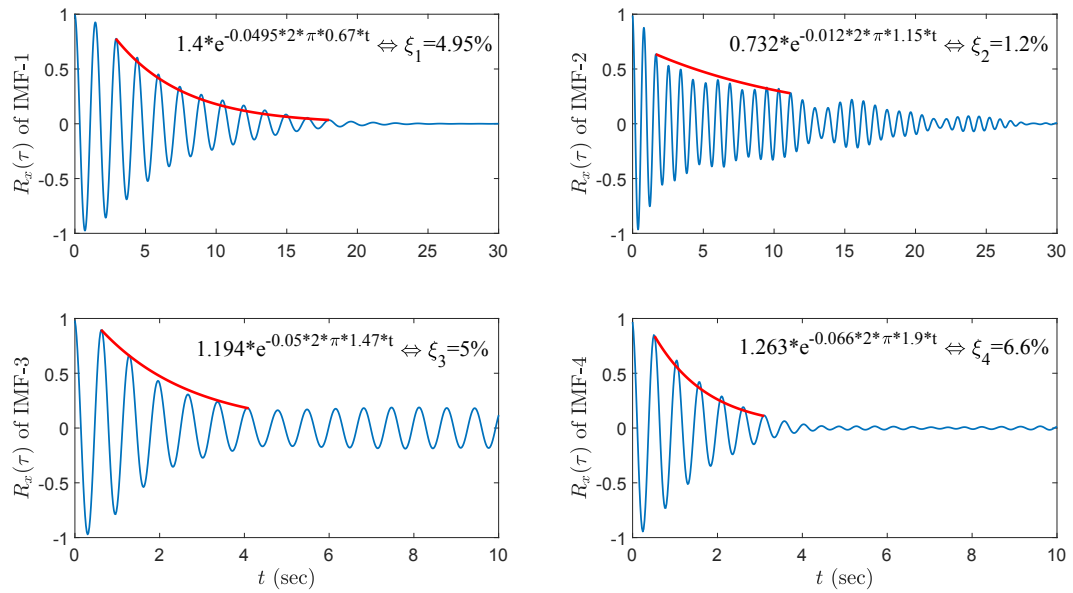


Figure 3.22: Damping ratio of the resulting modal responses the of the 4th floor measurement

3.3 10-DOF Model

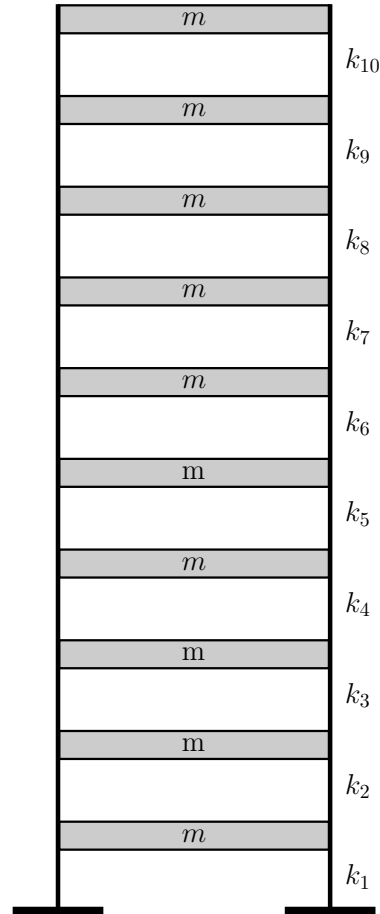


Figure 3.23: 10-DOF model

A simulation study is performed on a 10-storey model as shown in Fig. 3.23. The lumped mass of each floor is assumed to be 1 kg and the stiffness from k_1 to k_{10} are 175, 350, 525, 700, 875, 1050, 1225, 1400, 1575, and 1750 N/m, respectively. The damping is assumed to be 2% in first two modes. The natural frequencies are obtained as 0.78, 1.8, 2.83, 3.88, 4.96, 6.08, 7.25, 8.49, 9.87 and 11.52 Hz. The model is excited by Imperial Valley earthquake at its base. Fig. 3.24 shows the Fourier spectra of three typical floor vibration measurements of this model. In order to demonstrate the performance of the proposed method, the TVF-EMD is utilized on the second

and fifth floor vibration measurements.

First, the TVF-EMD method is applied on the second floor vibration measurements and consecutively 137 IMFs are extracted. The RMS value is used to high energy modal response components of all IMFs and the result is shown in Fig. 3.25. Fig. 3.26 shows the cluster of frequencies of all IMFs while Fig. 3.27 shows the cluster of frequencies of IMFs that are above the mean RMS values. It can be observed that the frequency of first and eighth mode can not be found in Fig. 3.27 due to their low energy in second floor measurement. Fig. 3.28 shows the IMFs obtained from the second-floor vibration measurements by using the TVF-EMD method.

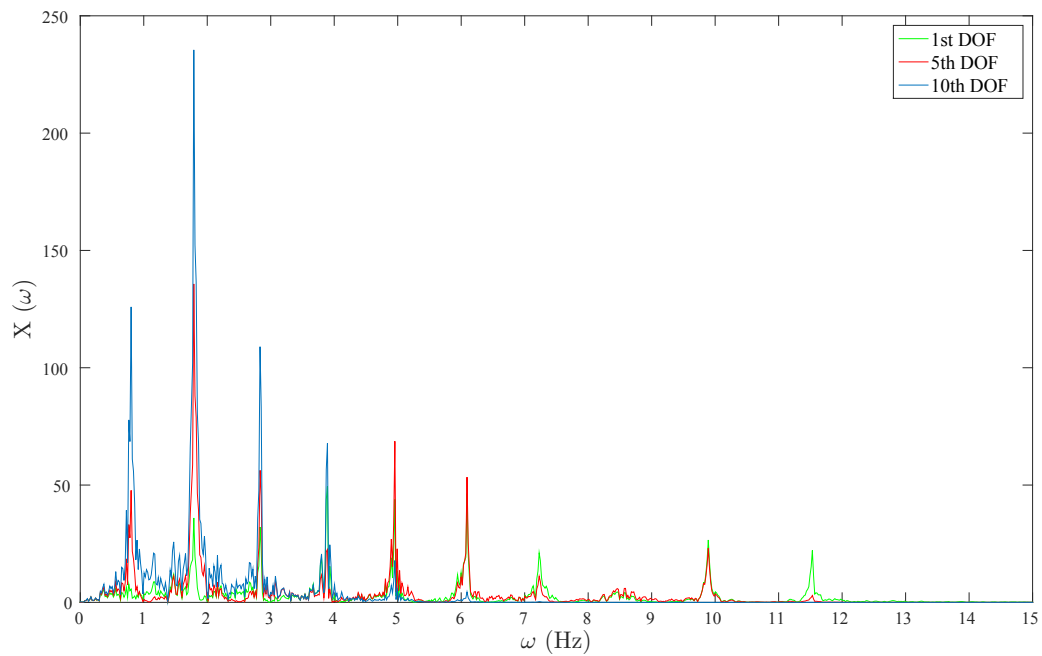


Figure 3.24: Fourier spectra of floor vibration measurements

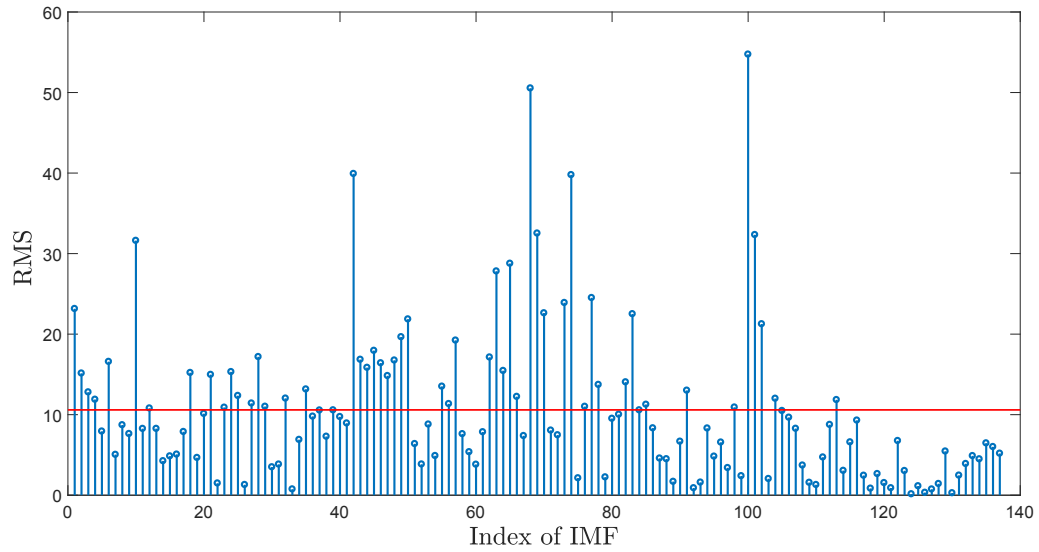


Figure 3.25: RMS values of IMFs of second floor measurement

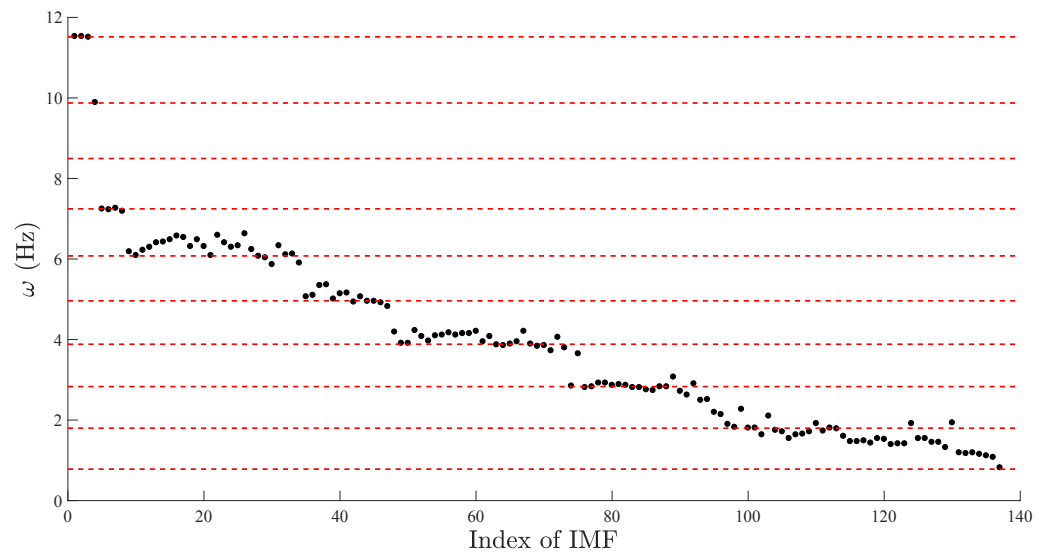


Figure 3.26: Cluster of frequencies of all IMFs

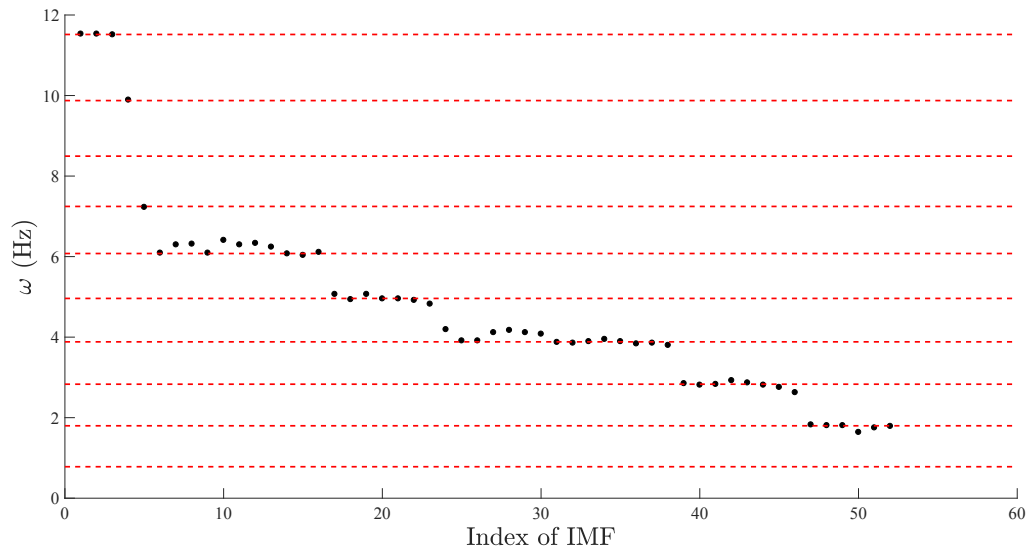


Figure 3.27: Cluster of frequencies of IMFs that are above μ_{rms}

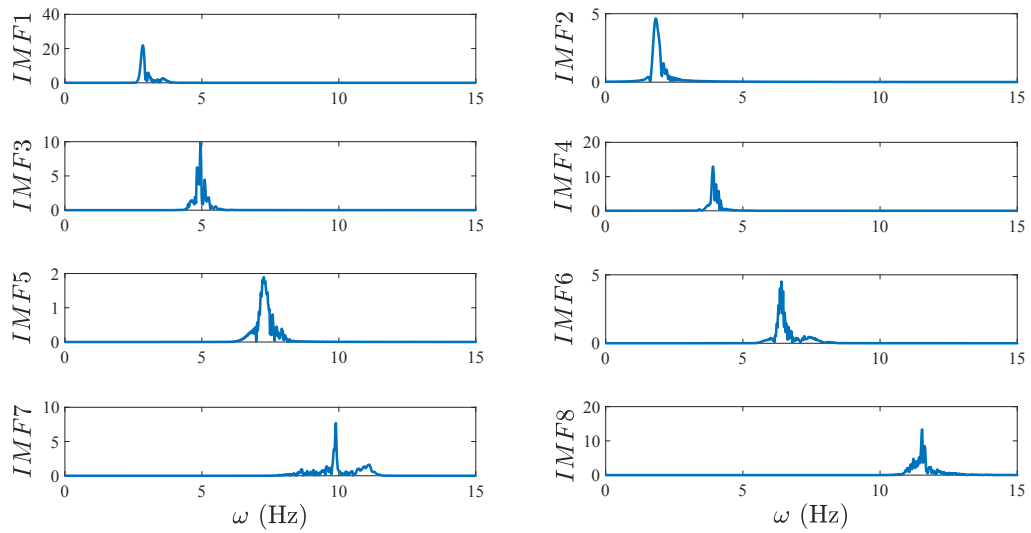


Figure 3.28: Fourier spectra of IMFs of the second floor measurement

The TVF-EMD is then applied to fifth floor vibration measurement and 195 IMFs are extracted using the proposed method. Then the RMS is applied to identify the low energy modes. The result is shown in Fig. 3.29. Fig. 3.30 shows the frequencies of all IMFs by using scatter diagram. Fig. 3.31 shows the scatter diagram of cluster IMFs's frequencies that are above the mean RMS values. From the Fig. 3.30 and Fig. 3.31, it can be observed that the identified frequencies can be determined where there is no slope in scatter diagram. Fig. 3.32 shows the typical IMFs that obtained from TVF-EMD. It can be observed that the proposed method has successfully extracted the mono-component modal responses. Table 3.3 shows theoretical and identified results revealing the efficiency of the proposed method with large DOFs.

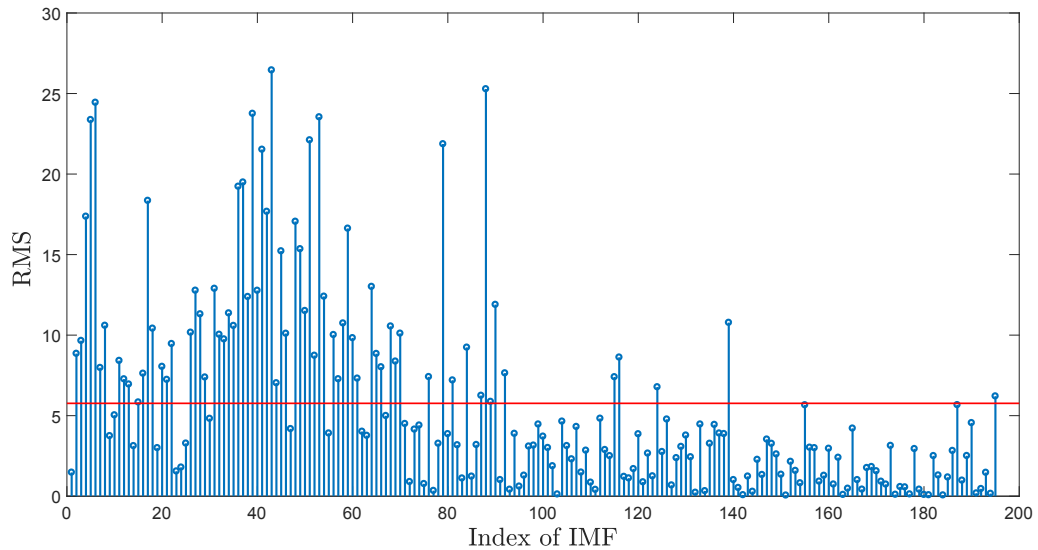


Figure 3.29: RMS values of IMFs of fifth floor measurement

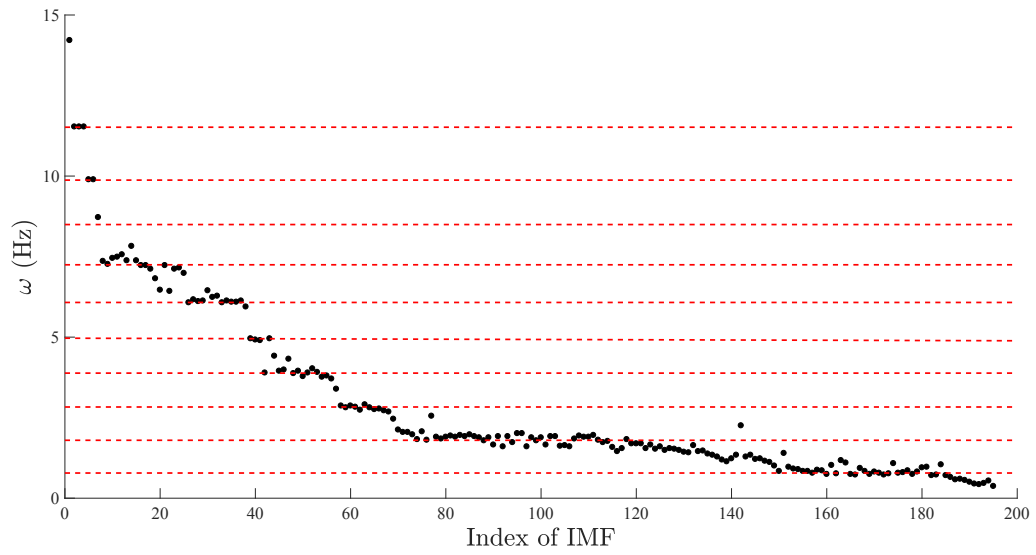


Figure 3.30: Cluster of frequencies of all IMFs

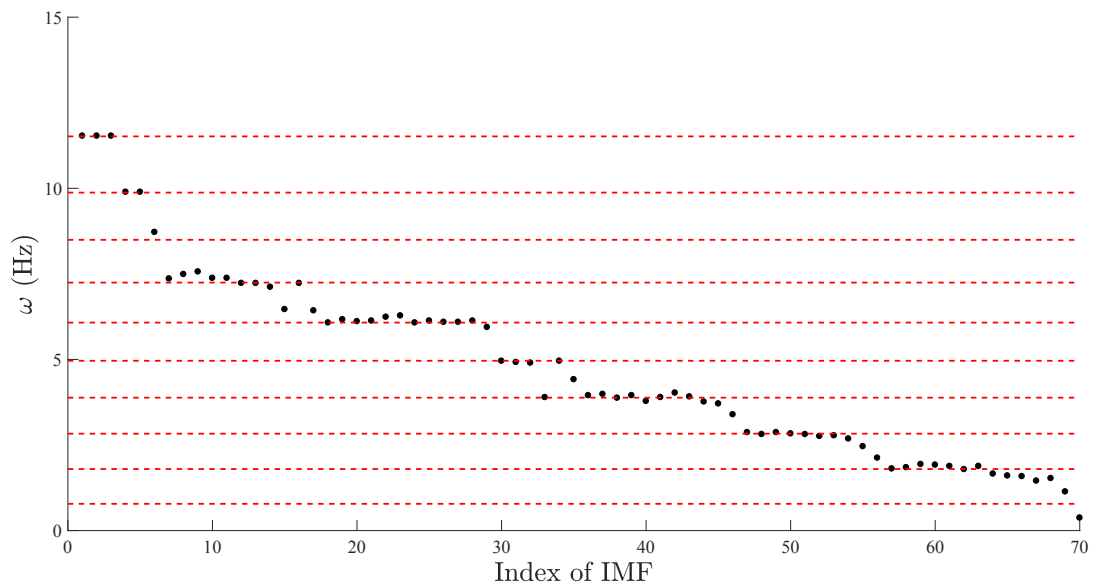


Figure 3.31: Cluster of frequencies of IMFs that are above μ_{rms}

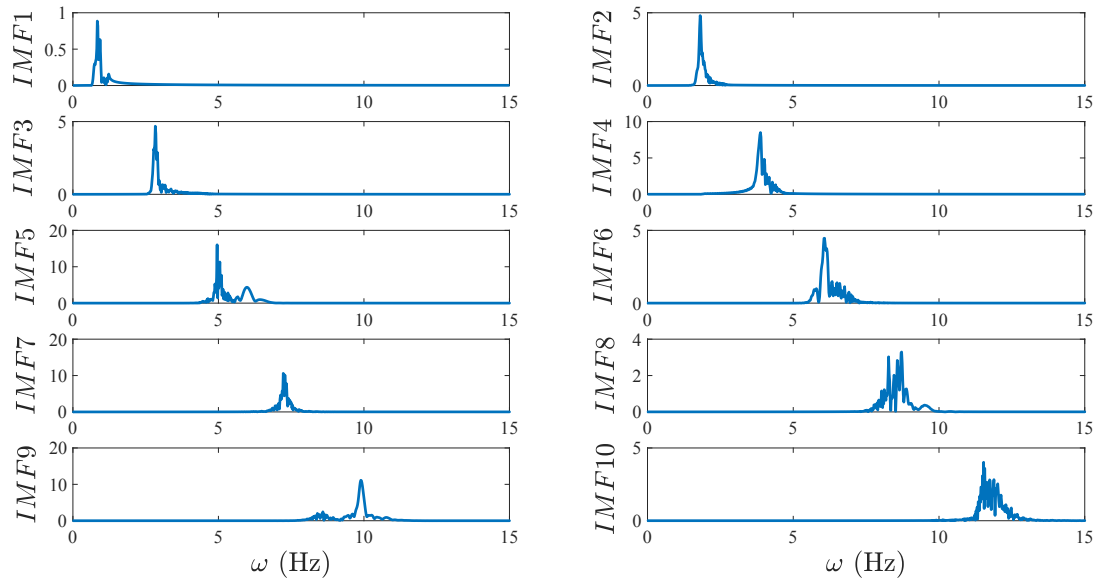


Figure 3.32: Fourier spectra of IMFs of the fifth floor

Table 3.3: Theoretical and identified modal parameters of second floor measurement

Mode #	1	2	3	4	5	6	7	8	9	10
ω_i (Hz)	0.78	1.8	2.83	3.88	4.96	6.08	7.25	8.49	9.87	11.52
$\hat{\omega}_i$ (Hz)	0.78	1.8	2.87	3.87	4.96	6.07	7.23	8.72	9.89	11.53
$\hat{\zeta}_i$ (%)	1.5	1	1	1.4	1.1	1.1	2.2	1.1	1	1.1

Chapter 4

Experimental and Full-scale Studies

In this chapter, the proposed method is validated using an experimental model and a footbridge bridge located at Lakehead University in Thunder Bay, Canada. In both studies, data collection is conducted in decentralized fashion such that only one sensor is available at a time. The proposed method is then employed over single channel vibration measurement and the identified results are compared with the Finite Element (FE) models.

4.1 Experimental Study

A six-story experimental model is used to validate the proposed method as shown in Fig. 4.1. The mass of first three floors is 2.47 kg each, and the other three floors have mass of 1.12 kg each, respectively. In order to apply dynamic load, the model is placed on a horizontal table which is connected to a shaker manufactured by Crystal InstrumentsTM. The top floor of the model is attached with a wired sensor which is acting as a reference sensor. On the other hand, a wireless sensor is utilized here as a mobile sensor which is roved over the structure across various DOFs during each subsequent data collection. The wireless sensor called NaradaTM manufactured by CivionicsTM is used in this experiment. As shown in Fig. 4.2 and 4.3, the Narada sensor has two components. One is the sensor unit which is attached to the DOF and the other unit is known as the base station which is responsible for collecting data

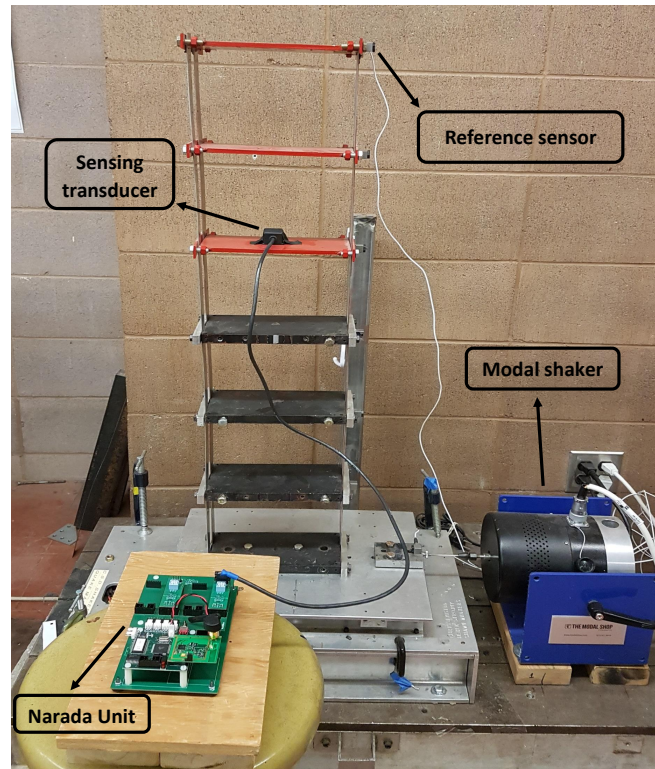


Figure 4.1: Experimental model

from the structure remotely. The details of these sensors can be found in [77]. A sampling frequency of 100 Hz is used for both wired and wireless sensors.



Figure 4.2: The Narada unit



Figure 4.3: The Narada base station

Once the setup is ready, the model is excited using a random shaking for 30 seconds via a control system attached to the modal shaker. The Narada sensor is

used to collect the data which are transferred to the Narada base by the Narada unit. Same steps are used to collect data from each floor, and Fig. 4.4 shows the position of Narada sensor on different floors in a decentralized manner. In this study, the data obtained from the second floor and fifth floor are used to demonstrate the results.

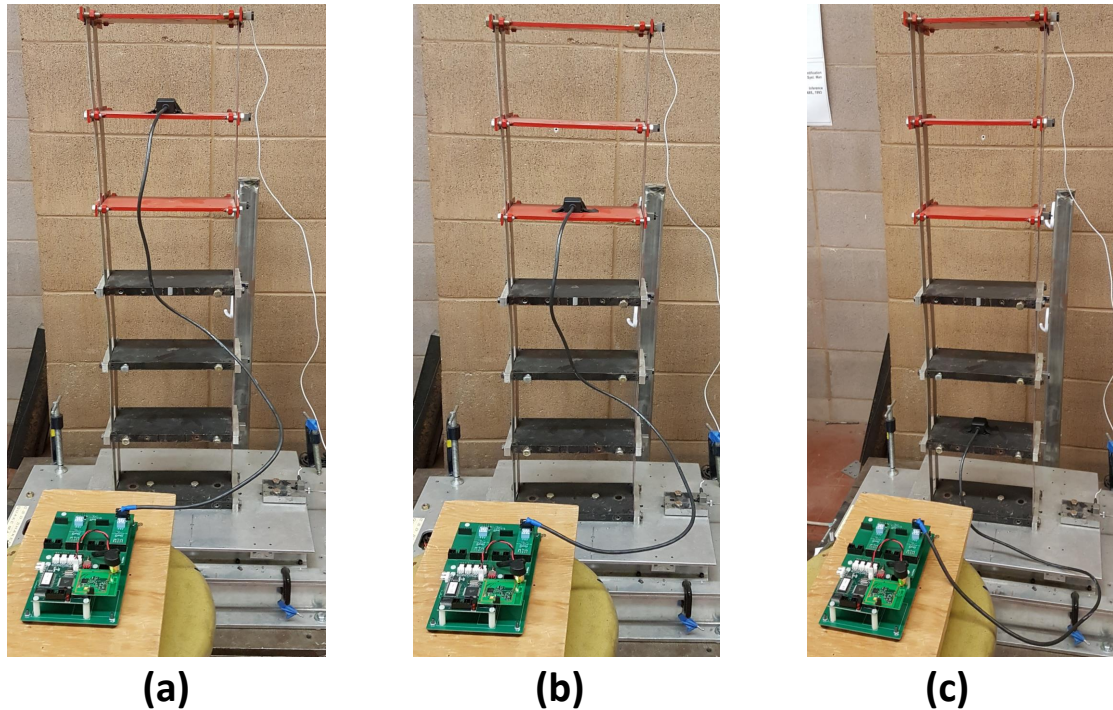


Figure 4.4: Mobile sensing where sensor is located at (a) 5th floor, (b) 4th floor and (c) 1st floor

Fig. 4.5 shows the Fourier spectra of the second floor measurement. The TVF-EMD method is first applied on the second floor vibration measurement and 250 IMFs are extracted by the proposed method. The RMS value is utilized to extract the key vibration modes and the result is shown in Fig. 4.6. Fig. 4.7 shows the cluster of frequencies of all IMFs. Fig. 4.8 shows typical IMFs obtained from the TVF-EMD. It can be observed that the proposed method has successfully extracted the mono-component modal responses.

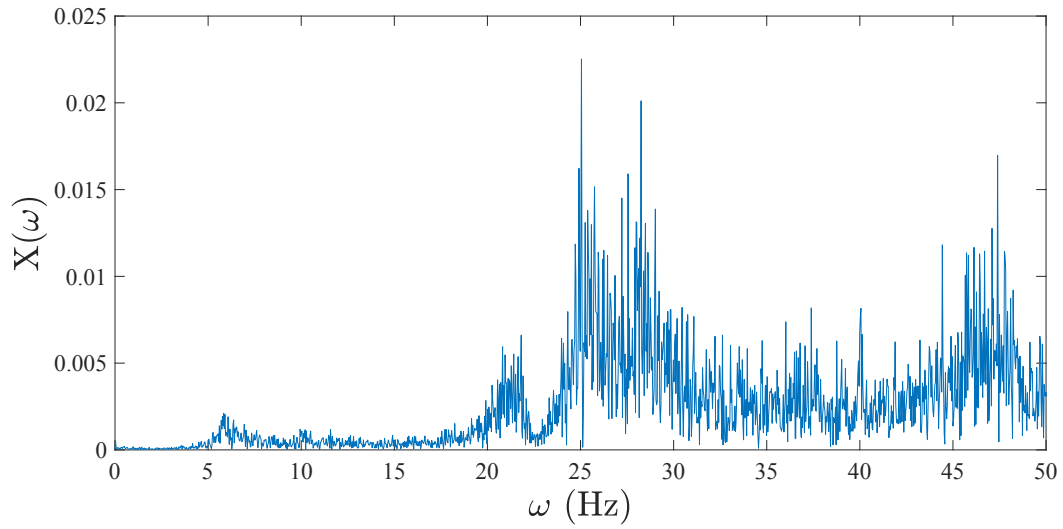


Figure 4.5: Fourier spectra of second floor vibration measurement

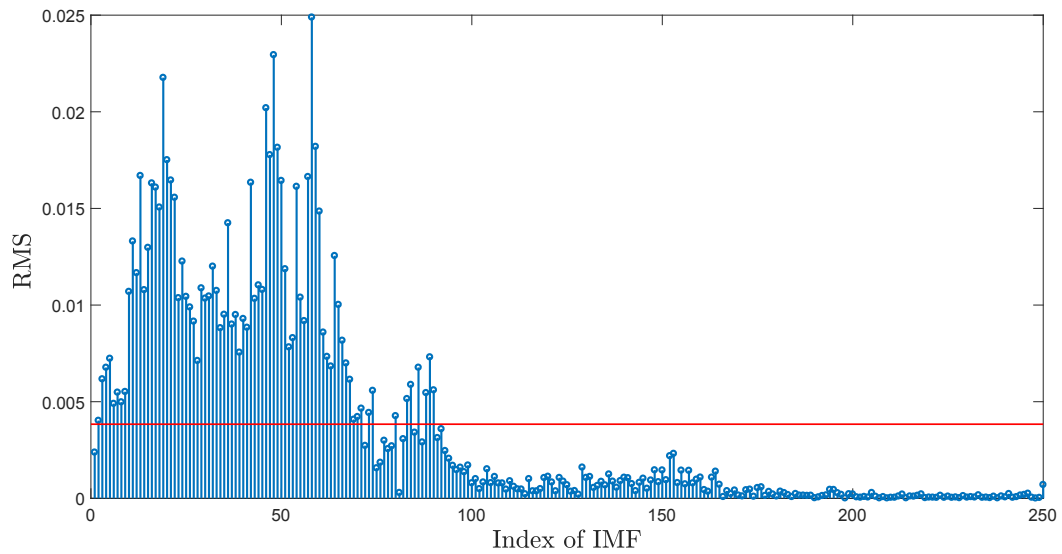


Figure 4.6: RMS values of IMFs of the second floor measurement

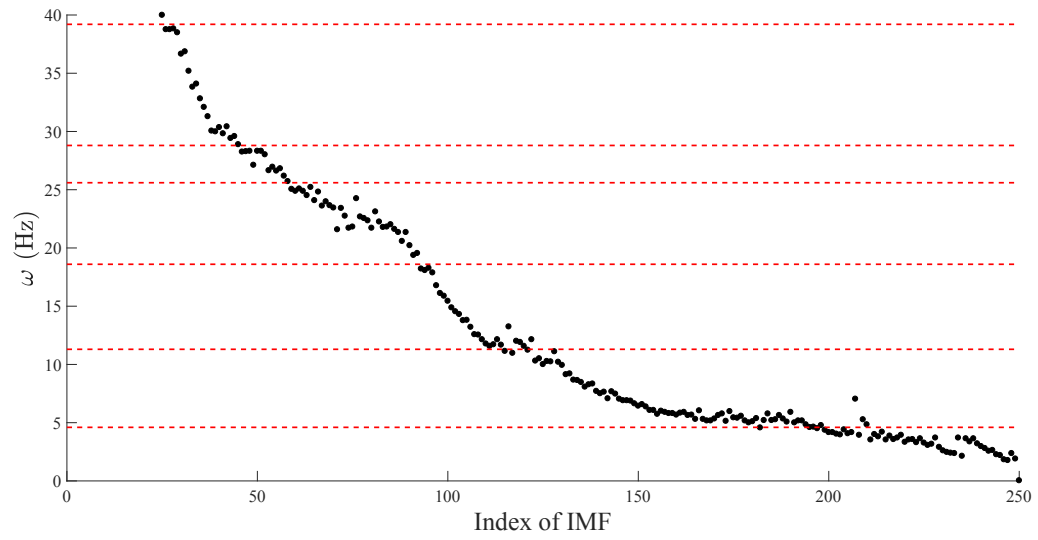


Figure 4.7: Cluster of frequencies of all IMF's

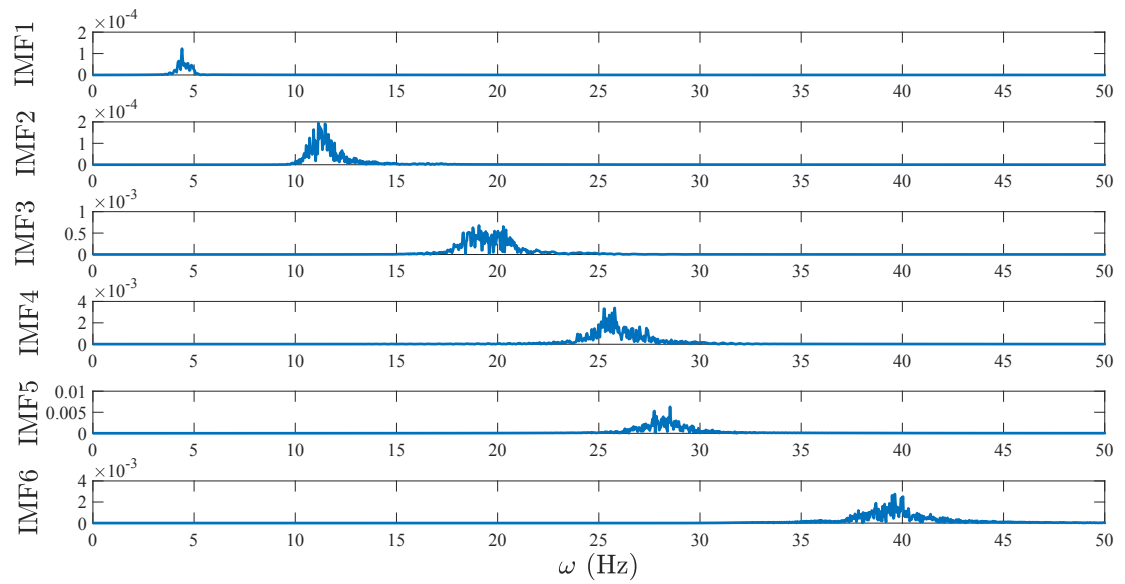


Figure 4.8: IMF's of the second floor measurement

The results of the fifth floor vibration measurement give 250 IMFs. As aforementioned, the RMS is utilized to extract higher energy modes and the result is shown in Fig. 4.9. Fig. 4.10 shows the scatter diagram of all IMFs frequencies. Fig. 4.11 shows the IMFs obtained from the fifth floor vibration measurements by using the TVF-EMD method. It can be observed that the proposed method has successfully extracted the mono-component components modal responses. Based on the known mass and stiffness, an analytical dynamical model is developed for this experimental system from which the theoretical frequencies are extracted. Table 4.1 shows Theoretical and identified results revealing the efficiency of the proposed method using real vibration data.

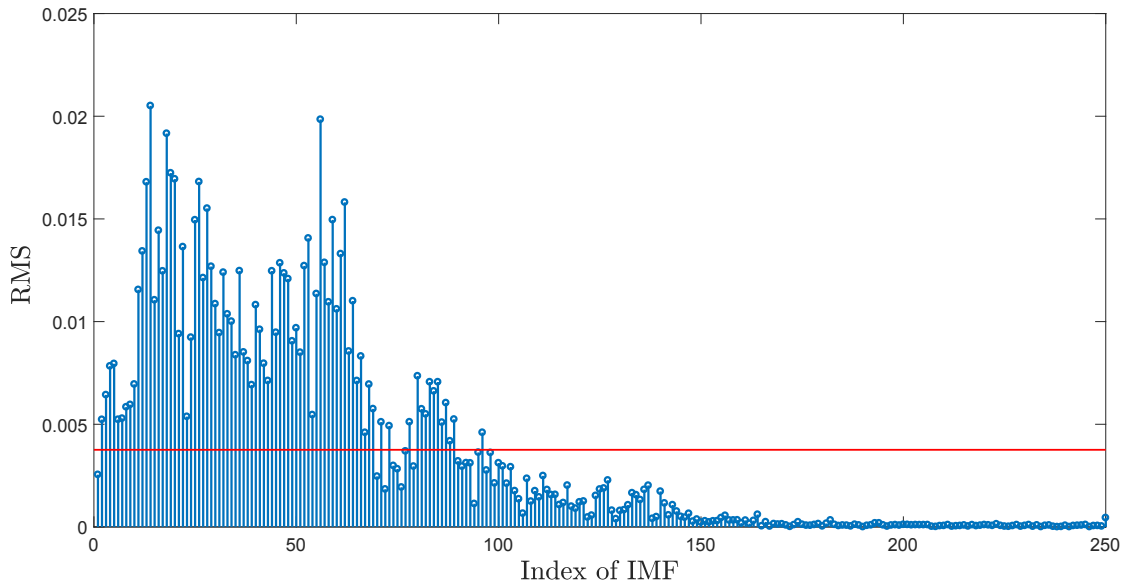


Figure 4.9: RMS values of IMFs of the fifth floor measurement

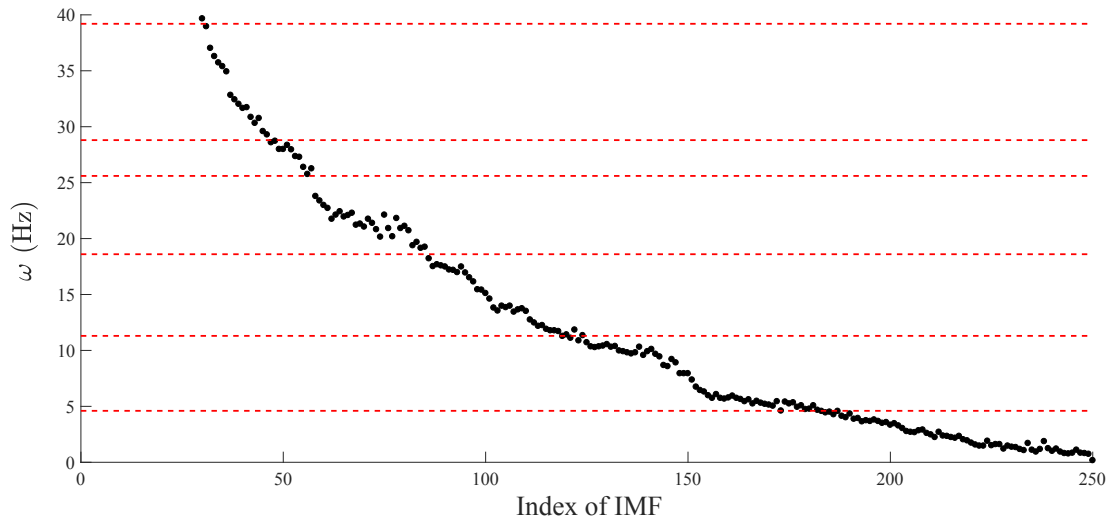


Figure 4.10: Cluster of frequencies of all IMFs

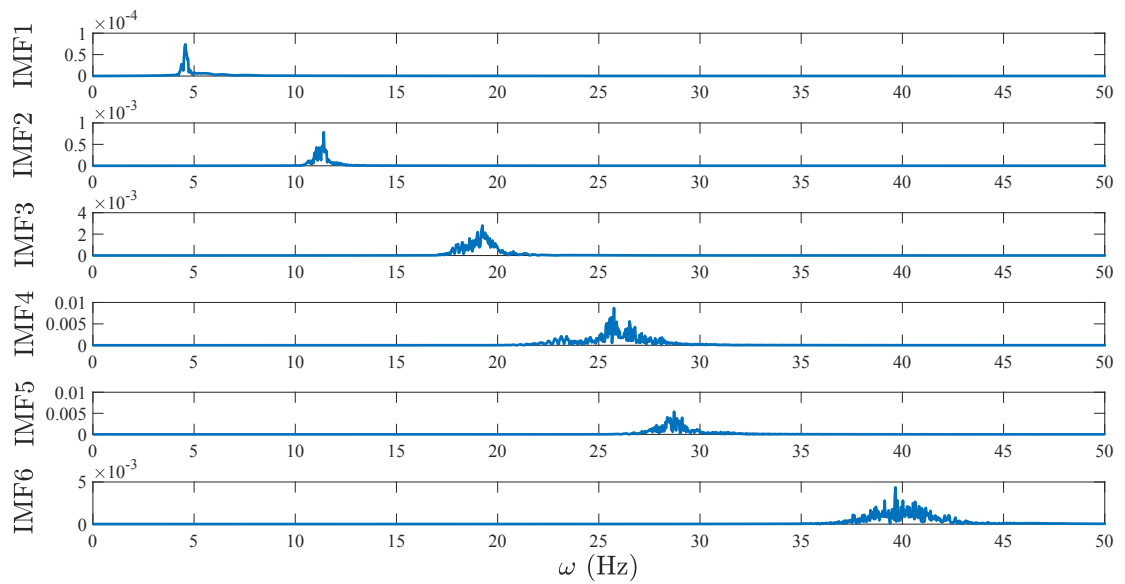


Figure 4.11: Fourier spectra of IMFs of the fifth floor measurement

Table 4.1: Theoretical and identified modal parameters of the experimental model

Mode #	1	2	3	4	5	6
ω_i (Hz)	4.6	11.3	18.6	25.6	28.8	39.2
$\hat{\omega}_i$ (Hz)	4.6	11.2	18.8	25.7	28.7	39.7
$\hat{\zeta}_i$ (%)	0.1	0.52	0.73	0.83	0.32	0.053

4.2 Full-scale Study

In this section, a footbridge located on the campus of Lakehead University is utilized for the implementation of the proposed method.



Figure 4.12: Pedestrian bridge on the campus of Lakehead University instrumented with wireless sensors

The pedestrian bridge crossing the McIntyre River on the campus of Lakehead

University is shown in Fig. 4.12. The bridge was built in 1967 and is supported by concrete piers at in each end, and is connected by steel struts spaced equally along the length of the bridge and wooden lumber for decking. During the test, sensors were mounted along the bridge to measure the bridge acceleration across a variety of locations and directions. Eight uniaxial wired sensors and six uniaxial wireless sensors were placed along the bridge to measure vertical acceleration, two uniaxial wired sensors were placed near the bridge to measure lateral acceleration and one triaxial sensor was placed at midspan to detect acceleration along all three axes.

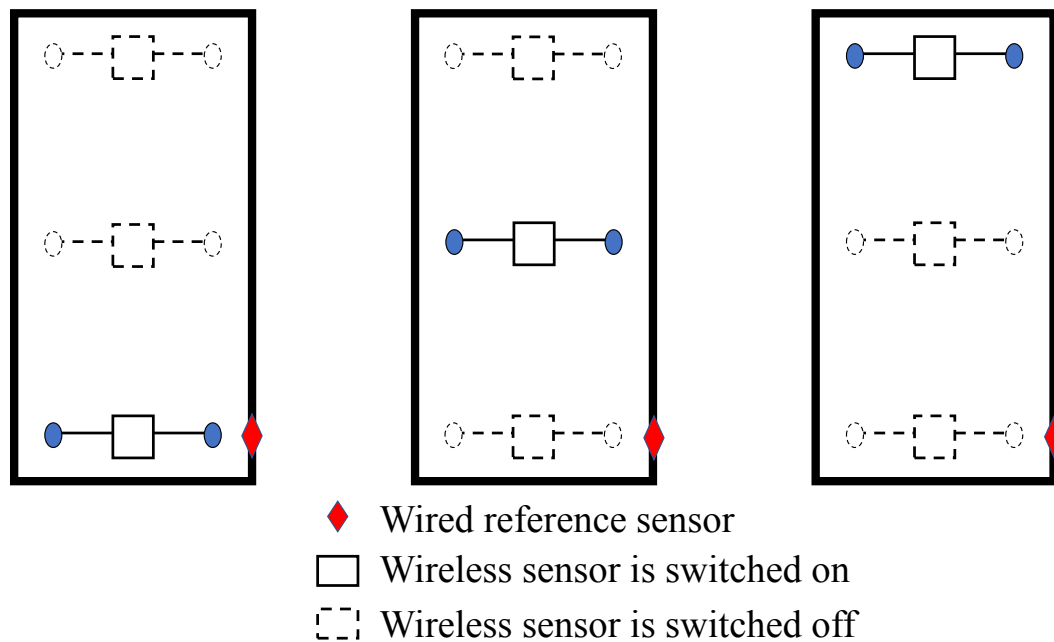


Figure 4.13: Decentralized implementation of sensors placed along the footbridge

In order to implement the mobile sensing technique, the Narada units are utilized in the similar fashion as it was done in the previous chapter. The decentralized sensor placement is illustrated in Fig. 4.13. Although three wireless sensors were placed, only one sensor was switched on during each test which was equivalent to decentralized moving sensing network where a single sensor is roved along the structure. Once the

instrumentation is completed, the bridge was subjected to a wide range of pedestrian excitation including walking, running and jogging. In this thesis, the wireless node that was placed in the middle of the bridge as shown in Fig. 4.14 is utilized.



Figure 4.14: The Narada unit at the mid-span of the bridge

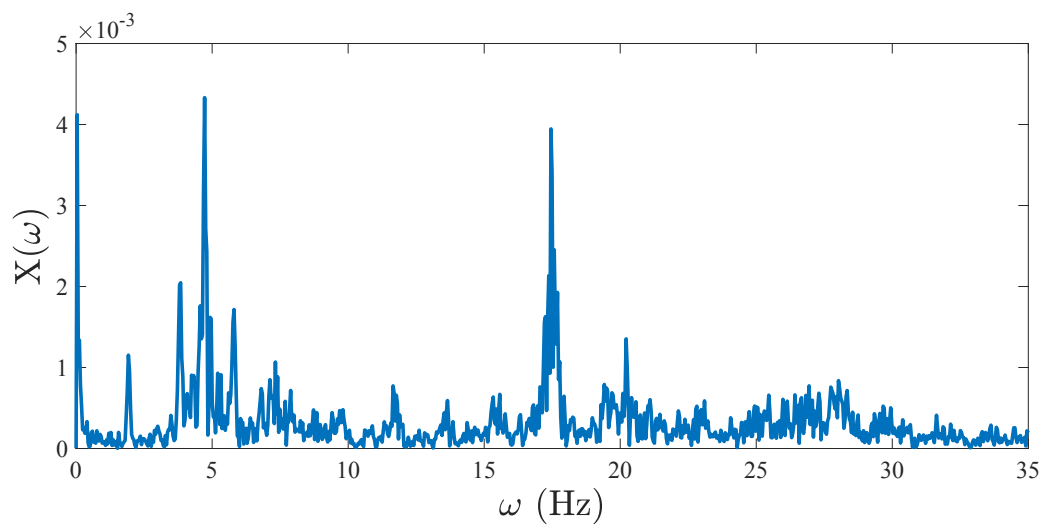


Figure 4.15: Fourier spectra of bridge vibration measurement

Fig. 4.15 shows the Fourier spectra of vibration measurement. Then, 250 IMFs are obtained from TVF-EMD method as shown in Fig. 4.16. Fig. 4.17 shows the cluster diagram of all IMFs frequencies. In Fig. 4.17, it can be observed that the actual frequencies can be determined from the scatter diagram by observing their slopes.

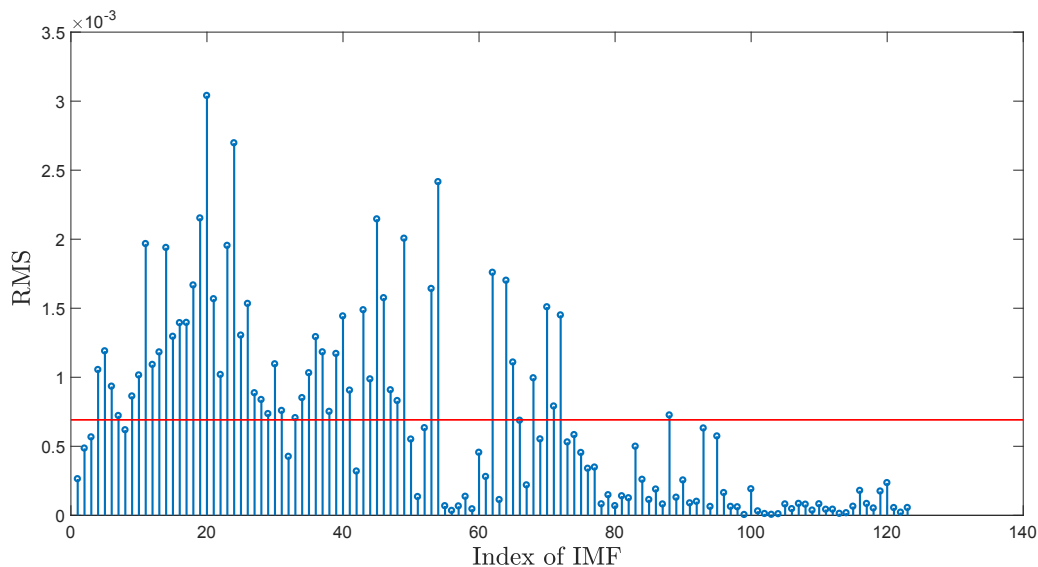


Figure 4.16: RMS values of IMFs of the mid-span measurement

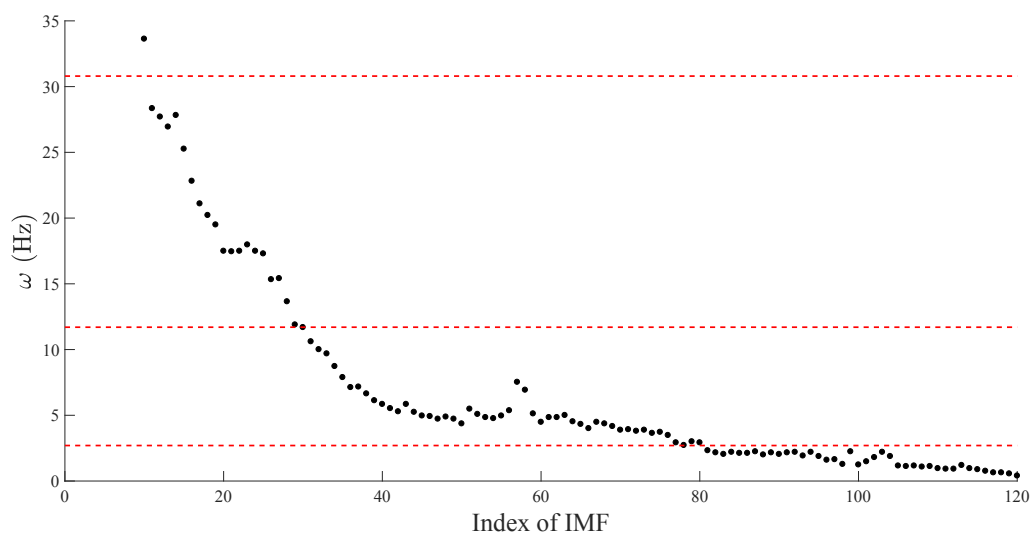


Figure 4.17: Cluster of frequencies of all IMFs

In order to validate the accuracy of the results, the structural plans of the pedestrian bridge are used to create a finite element model (FE) using S-FrameTM, and this model is subjected to unstressed vibration analysis to predict its mode shapes and natural frequencies. The main structural elements of the bridge are replicated in the software and mass of the wooden deck and other non-structural elements is estimated and applied to the structure as a uniformly distributed load. The bridge is assumed to consist of two main beams fixed on both ends, and thirteen cross bracing beams between them. Fig. 4.18 shows FE model and its mode shapes whereas Fig. 4.19 shows the typical IMFs obtained from TVF-EMD. The proposed method has successfully extracted the mono-component modal responses. After finding the modal responses by using the proposed method, auto-correlation function of modal responses is used to extract modal damping ratio. Fig. 4.20 shows the estimation of damping ratio as obtained from the IMFs of bridge vibration measurement. Table 4.2 shows theoretical and identified results revealing the efficiency of the proposed method using real vibration data.

Table 4.2: Theoretical and identified modal parameters of the footbridge

Mode #	1	2	3
ω_i (Hz)	2.7	11.7	30.8
$\hat{\omega}_i$ (Hz)	2.7	11.7	27.7
$\hat{\zeta}_i$ (%)	1.1	0.6	1.3

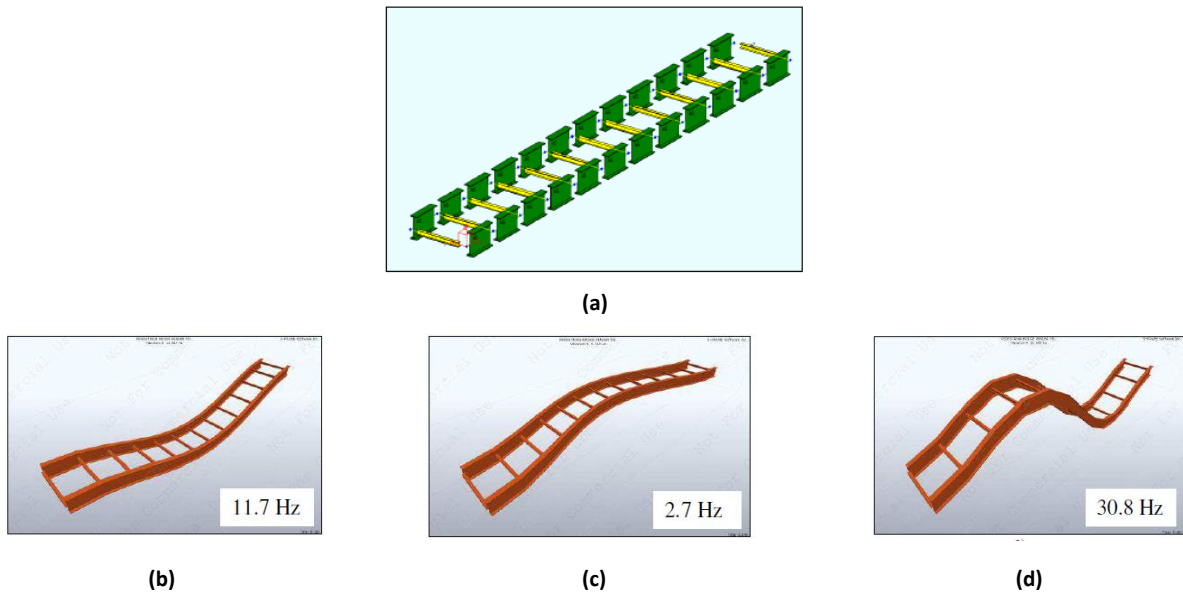


Figure 4.18: FE model and its mode shapes

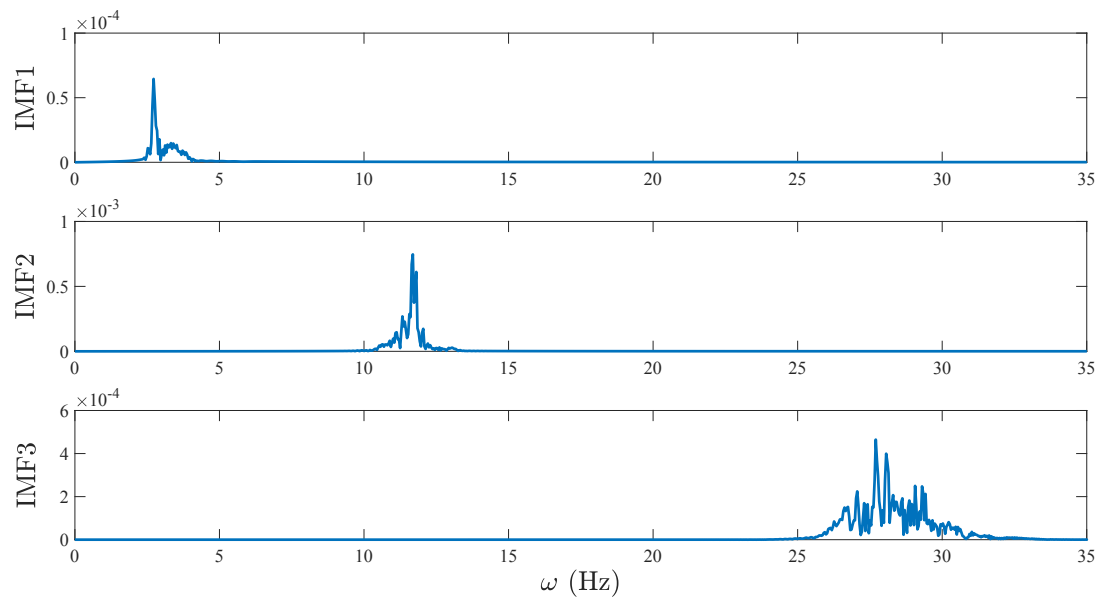


Figure 4.19: IMFs of the mid-span vibration measurement

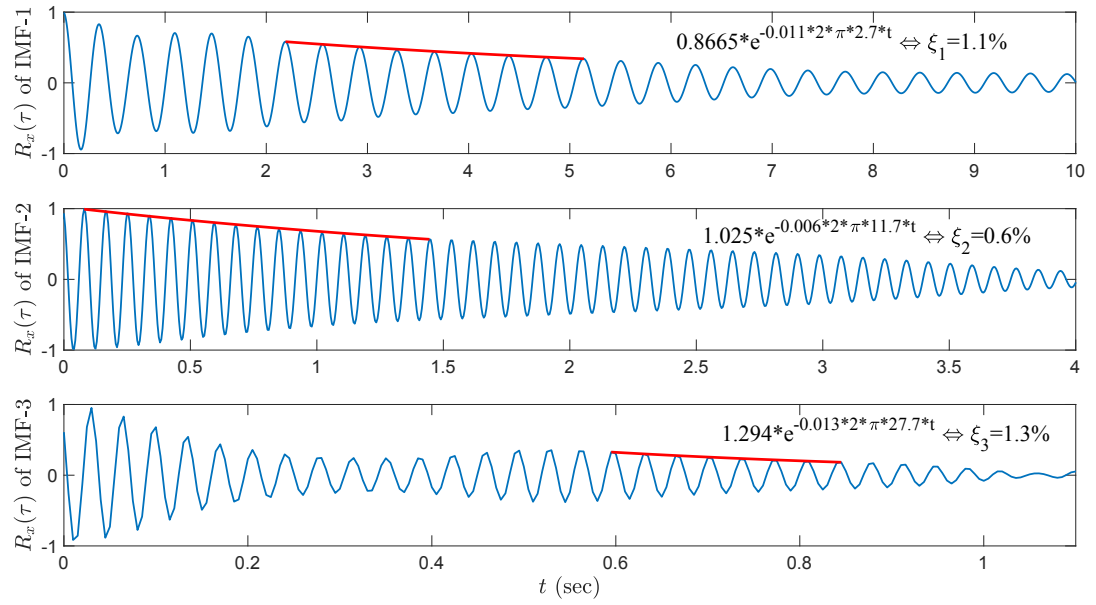


Figure 4.20: Damping ratio of the resulting modal responses of bridge

Chapter 5

Conclusions and Recommendations

In this Chapter, the conclusions of this thesis are summarized followed by the key research contributions. Finally, several recommendations are made for possible future work to contribute further in this area.

5.1 Conclusions

- The TVF-EMD method is explored for the *first time* as a potential system identification tool.
- The proposed method is free of any basis function, is data-driven in nature and suitable to perform modal identification using only a single sensor measurement.
- The TVF-EMD can correctly extract dominant modes without any mode-mixing.
- The results show improved performance of EMD under measurement noise and closely-spaced frequencies. The proposed method is validated through a suite of numerical studies employing a broad class of dynamical models and excitation characteristics.
- The practicability of the proposed method is verified within the framework of wireless decentralized framework in an laboratory model as well as a full-scale pedestrian bridge.

5.2 Major Contributions

The proposed research presented in this thesis has resulted in one conference paper and a journal paper (under review).

- **Lazhari, M.**, Sony, S., and Sadhu, A. (2018). “A newer time-frequency decomposition-based modal identification technique for structures.” **CSCE Structures Specialty Conference**, Fredericton, Ontario, Canada, (under review).
- **Lazhari, M.** and Sadhu, A. (2018). “Decentralized modal identification of structures using an adaptive empirical mode decomposition method.” **Journal of Sound and Vibration**, under review.

5.3 Future Work

Even through all the specific objectives of thesis are met, following future research is recommended to enhance the capability of existing mobile sensing-based SHM strategy using the TVF-EMD method.

- In this thesis, with the absence of any robotic vehicle, the decentralized sensing network is simulated through manual movement of wireless sensor from one place to another DOF. Such approach does not take into account the effect of sensor-vehicle interaction. It is proposed to expand this research considering a smart robotic device for data collection and data processing, and validate the accuracy of the proposed method.
- This method could be explored for damage detection where the structures are subjected to both discrete and progressive damages. Single sensor-based damage

detection method would be beneficial for the SHM community.

- The proposed method will be automated to develop a software such that any novice structural engineer can easily deploy this algorithm as a tool in real-time applications. Further efforts will be made to embed the algorithm into wireless sensors attached with the mobile robot.
- The applicability of this method needs to be investigated in identifying torsional modes.

Bibliography

- [1] Klikowicz, P., Salamak, M. and Poprawa, G. (2016). “Structural health monitoring of Urban Structures.” *Procedia Engineering*, 161, 958-962.
- [2] Reynders, E. (2012). “System identification methods for (operational) modal analysis: review and comparison.” *Archives of Computational Methods in Engineering*, 19(1).
- [3] Lynch, J. P. (2006). (2006). “A summary review of wireless sensors and sensor networks for structural health monitoring.” *The Shock and Vibration Digest*, 38(2), 91-128.
- [4] Zhu, D., Guo, J., Cho, C., Wang, Y., and Lee, K. M. (2012). “A wireless mobile sensor network for the system identification of a space frame bridge.” *IEEE/ASME Transactions on Mechatronics*, 17(3), 499-507.
- [5] Sadhu, A. (2013). “Decentralized ambient modal identification of structures.” *PhD Thesis*, Department of Civil and Environmental Engineering, University of Waterloo, Canada.
- [6] Guo, S., Zhang, X., Zhang, J., Zhou, Y., Moon, F., and Aktan, A. E. (2018). “Mobile impact testing of a simply-supported steel stringer bridge with reference-free measurement.” *Engineering Structures*, 159, 66-74.
- [7] Tche, F., Fischer, W., Caprari, G., Siegwart, R., Moser, R., and Mondada, F. (2009). “Magnebike: A magnetic wheeled robot with high mobility for inspecting complex-shaped structures.” *Journal of Field Robotics*, 26(5), 453-476.
- [8] Choi, C., Park, B., and Jung, S. (2010). “The design and analysis of a feeder pipe inspection robot with an automatic pipe tracking system.” *IEEE/ASME Transactions on Mechatronics*, 15(5), 736-745.
- [9] Murphy, M. P., and Sitti, M. (2007). “Waalbot: an agile small-scale wall-climbing robot utilizing dry elastomer adhesives.” *IEEE/ASME Transactions on Mechatronics*, 12(3), 330-338.
- [10] Provancher, W. R., Jensen-Segal, S. I., and Fehlberg, M. A. (2011). “ROCR: an energy-efficient dynamic wall-climbing robot.” *IEEE/ASME Transactions on Mechatronics*, 16(5), 897-906.
- [11] Huston, D. R., Esser, B., Gaida, G., Arms, S. W., and Townsend, C. P. (2001). “Wireless inspection of structures aided by robots.” *SPIE 4337, Health Monitoring and Management of Civil Infrastructure Systems, Newport Beach*, 147-154.

- [12] Backes, P., Bar-Cohen, Y., and Joffe, B. (n.d.). (1997). “The multifunction automated crawling system (MACS).” *Proceedings of International Conference on Robotics and Automation*, 335-340.
- [13] Todd, M., Mascarenas, D., Flynn, E., Rosing, T., Lee, B., Musiani, D., Dasgupta, S., Kpotufe, S., Hsu, D., Gupta, R., Park, G., Overly, T., Nothnagel, M., and Farrar, C. (2007). “A different approach to sensor networking for SHM: powering and interrogation with unmanned aerial vehicles.” *presented at the 6th Int. Workshop Structural Health Monitoring, Stanford, CA*.
- [14] Marulanda, J., Caicedo, J. M., and Thomson, P. (2017). “Modal identification using mobile sensors under ambient excitation.” *Journal of Computing in Civil Engineering*, 31(2), 04016051.
- [15] Wang, W., Joshi, A., Tirpankar, N., Erickson, P., Cline, M., Thangaraj, P., and Henderson, T. C. (2015). “Bayesian computational sensor networks: small-scale structural health monitoring.” *Procedia Computer Science*, 51, 2603-2612.
- [16] Lorenc, S. J., Handlon, B. E., and Bernold, L. E. (2000). “Development of a robotic bridge maintenance system.” *Automation in Construction*, vol. 9, pp. 251258.
- [17] Tung, P. C., Hwang, Y. R., and Wu, M. C. (2002). “The development of a mobile manipulator imaging system for bridge crack inspection.” *Automation in Construction*, vol. 11, pp. 717729.
- [18] Oh, J. K., Jang, G., Oh, S., Lee, J. H., Yi, B. J., Moon, Y. S., Lee, J. S., and Choi, Y. (2009). “Bridge inspection robot system with machine vision.” *Automation in Construction*, vol. 18, pp. 929941.
- [19] Zhu, D., Yi, X., Wang, Y., Lee, K.-M., and Guo, J. (2010). “A mobile sensing system for structural health monitoring: design and validation.” *Smart Materials and Structures*, 19,55011.
- [20] Lim, R. S., La, H. M., Shan, Z., and Sheng, W. (2011). “Developing a crack inspection robot for bridge maintenance.” *in Proceedings of IEEE International Conference Robotics and Automation, Shanghai, China*, pp. 62886293.
- [21] La, H. M., Lim, R. S., Basily, B., Gucunski, N., Yi, J., Maher, A., and Parvardeh, H. (2013) “Autonomous robotic system for high-efficiency non-destructive bridge deck inspection and evaluation.” *IEEE International Conference on Automation Science and Engineering (CASE)*, 19,55011.
- [22] Matarazzo, T. J. and Pakzad, S. N. (2016). “A mobile sensing system for structural health monitoring: design and validation.” *Structural Identification for mobile sensing with missing observation, Journal of Engineering Mechanics*, 18, 142(5), 118.

- [23] Goorts, K., Phillips, S., Ashasi-Sorkhabi, A., and Narasimhan, S. (2017). “Structural control using a deployable autonomous control system.” *International Journal of Intelligent Robotics and Applications*, 1(3), 306-326.
- [24] Astrom, K., and Eykhoff, P. (1971). “System identification A survey.” *Automatica*, 7(2), 123-162.
- [25] Ljung, L. (2010). “Perspectives on system identification.” *Annual Reviews in Control*, 34(1), 1-12.
- [26] Sette, S., and Boullart, L. (2001). “Genetic programming: principles and applications.” *Engineering Applications of Artificial Intelligence*, 14(6), 727-736.
- [27] Hazra, B. (2010). “Hybrid time and time-frequency blind source separation towards ambient system identification of structures.” *PhD Thesis*, Department of Civil and Environmental Engineering, University of Waterloo, Canada.
- [28] Maia, N. M. M. and et. al.(1997). “Theoretical and experimental modal analysis.” *Research Studies Press, Taunton, Somerset, UK*.
- [29] Spitznogle, F. R. and Quazi, A. H. (1970). “Representation and analysis of time limited signals using a complex exponential algorithm.” *The Journal of the Acoustical Society of America*, 47:1150–1155.
- [30] Ibrahim, S.R. and Mikulcik, E.C. (1973). “A time domain modal vibration test technique.” *Shock and Vibration Bulletin*, 43(4):21–37.
- [31] Allemang, R.J. and Brown, D.L.(1998). “A unified matrix polynomial approach to modal identification.” *Journal of Sound and Vibration*, 211(3):301–322.
- [32] Juang, J.N. and Pappa, R.S.(1985). “An eigen system realization algorithm for modal parameter identification and model reduction.” *Journal of Guidance, Control and Dynamics*, 8(5):620–627.
- [33] El-Kafafy, M., Guillaume, P., Peeters, B., Marra, F., and Coppotelli, G. (2012). “Advanced frequency-domain modal analysis for dealing with measurement noise and parameter uncertainty.” *Conference Proceedings of the Society for Experimental Mechanics Series*, pages 179–199.
- [34] Asmussen, J. C.(1997). “Modal analysis based on the random decrement technique application to civil engineering structures.” *PhD Thesis, Alborg university, Denmark*.
- [35] Lin, C. C., Wang, J. F. and Ueng, J.M.(2001). “Vibration control identification of seismically excited m.d.o.f. structure-ptmd systems.” *Journal of Sound and Vibration*, 240(1):87–115.

- [36] VanOverschee, P. and De Moor, B.(1993). “N4sid: numerical algorithms for state space subspace system identification” *Proceedings of the IFAC World Congress*, pages 361–364.
- [37] VanOverschee, P. and De Moor, B.(1996). “Subspace identification for linear systems: Theory, Implementation, Applications.” *Dordrecht, Netherlands*.
- [38] Ma, T., Yang, H. T., and Chang, C. (2005). “Structural Damage Diagnosis and Assessment under Seismic Excitations.” *Journal of Engineering Mechanics*, 131(10), 1036-1045.
- [39] Bagheri, A., Hosseinzadeh, A. Z., Rizzo, P., and Amiri, G. G. (2016). “Time domain damage localization and quantification in seismically excited structures using a limited number of sensors.” *Journal of Vibration and Control*, 23(18), 2942-2961.
- [40] Liu, G., Mao, Z., and Todd, M. (2016). “Damage detection using transient trajectories in phase-space with extended random decrement technique under non-stationary excitations.” *Smart Materials and Structures*, 25(11), 115014.
- [41] Zhong, K., and Chang, C. C. (2016). “Recursive combined subspace identification technique for tracking dynamic characteristics of structures under earthquake excitation.” *Journal of Engineering Mechanics*, 142(12), 04016092.
- [42] Richardson, M.H. and Formenti, D.L. (1982). “Parameter estimation from frequency response measurements using rational fraction polynomials.” *Proceedings of 1st IMAC Conference, Orlando, Florida*, pages 1–15.
- [43] Zhang, L., Kanda, H., Brown, L. D. and Allemang, J. R.(1985). “Frequency domain poly-reference method for modal analysis.” *Journal of Applied Mechanics*, ASME, 106(85).
- [44] Brincker, R., Zhang, L. and Anderson, P.(2001). “Modal identification of output-only systems using frequency domain decomposition.” *Smart Materials and Structures*, 10(3):441–445.
- [45] Brincker, R., Zhang, L. and Anderson, P.(2000). “Modal identification from ambient responses using frequency domain decomposition.” *In Proceedings of the International Modal Analysis Conference(IMAC)*, San Antonio, Texas, USA.
- [46] Tondreau, G., and Deraemaeker, A. (2014). “Automated data-based damage localization under ambient vibration using local modal filters and dynamic strain measurements: Experimental applications.” *Journal of Sound and Vibration*, 333(26), 7364-7385.
- [47] Valds-Gonzlez, J., De-La-Colina, J., and Gonzlez-Prez, C. A. (2014). “Experiments for seismic damage detection of a RC frame using ambient and forced vibration records.” *Structural Control and Health Monitoring*, 22(2), 330-346.

- [48] Figueiredo, E., Radu, L., Worden, K., and Farrar, C. R. (2014). “A Bayesian approach based on a Markov-chain Monte Carlo method for damage detection under unknown sources of variability.” *Engineering Structures*, 80, 1-10.
- [49] Ding, Y., Zhao, B., Wu, B., Xu, G., Lin, Q., Jiang, H., and Miao, Q. (2015). “A condition assessment method for time-variant structures with incomplete measurements.” *Mechanical Systems and Signal Processing*, 58-59, 228-244.
- [50] Adeli, H., Perez-Ramirez, C. A., Amezcuita-Sanchez, J. P., Valtierra-Rodriguez, M., Romero-Troncoso, R. D., Dominguez-Gonzalez, A., and Osornio-Rios, R. A. (2016). “Time-frequency techniques for modal parameters identification of civil structures from acquired dynamic signals.” *Journal of Vibroengineering*, 18(5), 3164-3185.
- [51] Sadhu, A., Narasimhan, S., and Antoni, J. (2017). “A review of output-only structural mode identification literature employing blind source separation methods.” *Mechanical Systems and Signal Processing*, 94, 415-431.
- [52] Hou, Z., Noori, M. and Amand, R. S. (2000). “Wavelet-based approach for structural damage detection.” *J. Engrg. Mech*, 126(7).
- [53] Huang, N. E., Shen, Z., Long, R., Wu, M. C., Shih, H. H., Zheng, Q., Yen, N-C., Tung, C. C. and Liu, H. H. (1998). “The empirical mode decomposition and the Hilbert spectrum for nonlinear and non-stationary time series analysis.” *Proceedings of the Royal Society A: Mathematical, Physical and Engineering Sciences*, 454.1971, 903-995.
- [54] Rilling, G., Flandrin, P., Goncalves, P. (2003). “On empirical mode decomposition and its algorithms.” *In: IEEE-EURASIP workshop on nonlinear signal and image processing NSIP-03*, Grado (I).
- [55] Li, H., Li, Z., and Mo, W. (2017). “A time varying filter approach for empirical mode decomposition.” *Signal Processing*, 138, 146-158.
- [56] Qin, S., Wang, Q., and Kang, J. (2015). “Output-only modal analysis based on improved empirical mode decomposition method.” *Advances in Materials Science and Engineering*, 2015, 1-12.
- [57] Song, X., Ma, H., and Wang, K. (2017). “A new developed modal parameter identification method based on empirical mode decomposition and natural excitation technique.” *Procedia Engineering*, 199, 1020-1025.
- [58] Moore, K. J., Kurt, M., Eriten, M., Mcfarland, D. M., Bergman, L. A., and Vakakis, A. F. (2018). “Wavelet-bounded empirical mode decomposition for measured time series analysis.” *Mechanical Systems and Signal Processing*, 99, 14-29.

- [59] Zhang, X., Du, X., and Brownjohn, J. (2012). “Frequency modulated empirical mode decomposition method for the identification of instantaneous modal parameters of aeroelastic systems.” *Journal of Wind Engineering and Industrial Aerodynamics*, 101, 43-52.
- [60] Geng, C., Wang, F., Zhang, J., and Jin, Z. (2014). “Modal parameters identification of power transformer winding based on improved Empirical Mode Decomposition method.” *Electric Power Systems Research*, 108, 331-339.
- [61] He, X., Hua, X., Chen, Z., and Huang, F. (2011). “EMD-based random decrement technique for modal parameter identification of an existing railway bridge.” *Engineering Structures*, 33(4), 1348-1356.
- [62] Yang, Y., and Chang, K. (2009). “Extraction of bridge frequencies from the dynamic response of a passing vehicle enhanced by the EMD technique.” *Journal of Sound and Vibration*, 322(4-5), 718-739.
- [63] Yu, D., and Ren, W. (2005). “EMD-based stochastic subspace identification of structures from operational vibration measurements.” *Engineering Structures*, 27(12), 1741-1751.
- [64] Bagheri, A., Ozbulut, O. E., and Harris, D. K. (2018). “Structural system identification based on variational mode decomposition.” *Journal of Sound and Vibration*, 417, 182-197.
- [65] Rehman, N. and Mandic, D. P. (2010). “Multivariate empirical mode decomposition.” *Proceedings of The Royal Society A*, 466, 1291–1302.
- [66] Syed, K. B. and Mohammed, I. H. B. (2016). “Classification of motor imagery movements using multivariate empirical mode decomposition and short time Fourier transform based hybrid method.” *Engineering Science and Technology, an International Journal*, 19, 457–464.
- [67] Rehman, N., Ehsan, S., Abdullah, S. M., Akhtar, M. J., Danilo, P. M. and Klaus, D. M. (2015). “Multi-scale pixel-based image fusion using multivariate empirical mode decomposition.” *Sensors*, 15, 10923–10947.
- [68] Sadhu, A. (2016). “An integrated multivariate empirical mode decomposition method towards modal identification of structures.” *Journal of Vibration and Control*, 23(17), 27272741.
- [69] Barbosh, M., Sadhu, A., and Vogrig, M. (2018). “Multisensor-based hybrid empirical mode decomposition method towards system identification of structures.” *Structural Control and Health Monitoring*.
- [70] Li, H., Deng, X., and Dai, H. (2007). “Structural damage detection using the combination method of EMD and wavelet analysis” *Mechanical Systems and Signal Processing*, 21(1), 298-306.

- [71] Xu, Y. L., and Chen, J. (2004). “Structural damage detection using empirical mode decomposition: experimental investigation.” *Journal of Engineering Mechanics*, 130(11), 1279-1288.
- [72] Pines, D., and Salvino, L. (2006). “Structural health monitoring using empirical mode decomposition and the Hilbert phase.” *Journal of Sound and Vibration*, 294(1-2), 97-124.
- [73] O'Brien, E. J., Malekjafarian, A., and Gonzalez, A. (2017). “Application of empirical mode decomposition to drive-by bridge damage detection.” *European Journal of Mechanics - A/Solids*, 61, 151-163.
- [74] Aied, H., Gonzalez, A., and Cantero, D. (2016). “Identification of sudden stiffness changes in the acceleration response of a bridge to moving loads using ensemble empirical mode decomposition.” *Mechanical Systems and Signal Processing*, 66-67, 314-338.
- [75] Guo, C., Wen, Y., Li, P., and Wen, J. (2016). “Adaptive noise cancellation based on EMD in water-supply pipeline leak detection. Measurement.” *Measurement*, 79, 188-197.
- [76] Flandrin, P., Rilling, G., and Goncalves, P. (2004). “Empirical mode decomposition as a filter bank.” *IEEE Signal Process Lett*, 11(2), 112114.
- [77] Lynch, J. P. (2007). “Empirical mode decomposition as a time-varying multi-rate signal processing system.” *Philosophical Transactions of the Royal Society A: Mathematical, Physical and Engineering Sciences*, 365(1851), 345-372.